

Cross sections for inelastic meson-meson scattering via quark-antiquark annihilation

Zhen-Yu Shen,¹ Xiao-Ming Xu,¹ and H. J. Weber²

¹Department of Physics, Shanghai University, Baoshan, Shanghai 200444, China

²Department of Physics, University of Virginia, Charlottesville, Virginia 22904, USA

(Received 13 December 2015; published 15 August 2016)

We study inelastic meson-meson scattering that is governed by quark-antiquark annihilation and creation involving a quark and an antiquark annihilating into a gluon, and subsequently the gluon creating another quark-antiquark pair. The resultant hadronic reactions include for $I = 1$: $\pi\pi \rightarrow \rho\rho$, $K\bar{K} \rightarrow K^*\bar{K}^*$, $K\bar{K}^* \rightarrow K^*\bar{K}^*$, $K^*\bar{K} \rightarrow K^*\bar{K}^*$, as well as $\pi\pi \rightarrow K\bar{K}$, $\pi\rho \rightarrow K\bar{K}^*$, $\pi\rho \rightarrow K^*\bar{K}$, and $K\bar{K} \rightarrow \rho\rho$. In each reaction, one or two Feynman diagrams are involved in the Born approximation. We derive formulas for the unpolarized cross section, the transition amplitude, and the transition potential for quark-antiquark annihilation and creation. The unpolarized cross sections for the reactions are calculated at six temperatures, and prominent temperature dependence is found. It is due to differences among mesonic temperature dependence in hadronic matter.

DOI: 10.1103/PhysRevD.94.034030

I. INTRODUCTION

All possible meson-meson scattering takes place in hadronic matter that is created in ultrarelativistic heavy-ion collisions. Yet, no hadronic meson beam collision experiments are possible. Therefore, we need to study meson-meson scattering theoretically. In Refs. [1,2] we have treated in the first Born approximation the quark interchange mechanism [3] in the endothermic nonresonant reactions $\pi\pi \rightarrow \rho\rho$ for $I = 2$, $KK \rightarrow K^*K^*$ for $I = 1$, $KK^* \rightarrow K^*K^*$ for $I = 1$, $\pi K \rightarrow \rho K^*$ for $I = 3/2$, $\pi K^* \rightarrow \rho K^*$ for $I = 3/2$, $\rho K \rightarrow \rho K^*$ for $I = 3/2$, and $\pi K^* \rightarrow \rho K$ for $I = 3/2$. In some regimes, these reactions are governed by quark interchange. Cross sections for these reactions change considerably with temperature of hadronic matter. For example, every reaction has a rising peak cross section when the temperature becomes critical. Clearly, meson-meson scattering in hadronic matter has interesting features that need to be studied.

Meson-meson scattering can be mediated not only by quark interchange but also by quark-antiquark annihilation and resonances. In the present work, we concentrate on meson-meson scattering that happens through quark-antiquark annihilation. Starting from an effective Lagrangian, cross sections for $\pi\pi \rightarrow K\bar{K}$, $\rho\rho \rightarrow K\bar{K}$, $\pi\rho \rightarrow K\bar{K}^*$, and $\pi\rho \rightarrow K^*\bar{K}$ in vacuum through one-meson exchange have been obtained in Ref. [4]. Many other reactions are also possible in hadronic matter. Here we consider not only the four reactions $\pi\pi \rightarrow K\bar{K}$, $K\bar{K} \rightarrow \rho\rho$, $\pi\rho \rightarrow K\bar{K}^*$, and $\pi\rho \rightarrow K^*\bar{K}$, but also $K\bar{K} \rightarrow K^*\bar{K}^*$, $K\bar{K}^* \rightarrow K^*\bar{K}^*$, $K^*\bar{K} \rightarrow K^*\bar{K}^*$, and $\pi\pi \rightarrow \rho\rho$ for $I = 1$, which are governed by quark-antiquark annihilation. These reactions are important in the evolution of hadronic matter created in ultrarelativistic heavy-ion collisions [5–7].

In the first Born approximation, we consider the annihilation of a quark-antiquark pair into a gluon and the creation of another quark-antiquark pair from the gluon. Gluon propagation has already been taken into account in $p\bar{p}$ annihilation into mesons. Different approximations to the gluon propagation have been made to derive transition potentials in Refs. [8–10]. These are the 3S_1 models. The $p\bar{p}$ annihilation into mesons has also been studied in the 3P_0 model where a quark and an antiquark annihilate into the vacuum and another quark-antiquark pair is created from the vacuum [11,12]. This nonperturbative mechanism is not considered here.

This paper is organized as follows. In Sec. II we derive the formulas of unpolarized cross section for meson-meson reactions that are governed by the annihilation and creation of a quark-antiquark pair. In Sec. III we derive a transition potential for the annihilation and creation of a quark-antiquark pair. In Sec. IV we present transition amplitudes and calculate color matrix elements, spin matrix elements, and flavor matrix elements. In Sec. V we provide mesonic quark-antiquark relative-motion wave functions. In Sec. VI we calculate elastic phase shifts for $\pi\pi$ scattering for $I = 0$ and $I = 1$, calculate unpolarized cross sections for nine channels of inelastic meson-meson scattering that is governed by quark-antiquark annihilation and creation, and give relevant discussions. In Sec. VII we summarize the present work.

II. CROSS-SECTION FORMULAS

If the quark q_1 of meson $A(q_1\bar{q}_1)$ has the same flavor as the antiquark \bar{q}_2 of meson $B(q_2\bar{q}_2)$ and/or the antiquark \bar{q}_1 and the quark q_2 have the same flavor, the reaction $A + B \rightarrow C + D$ may take place through quark-antiquark annihilation and creation as shown in Fig. 1. Corresponding

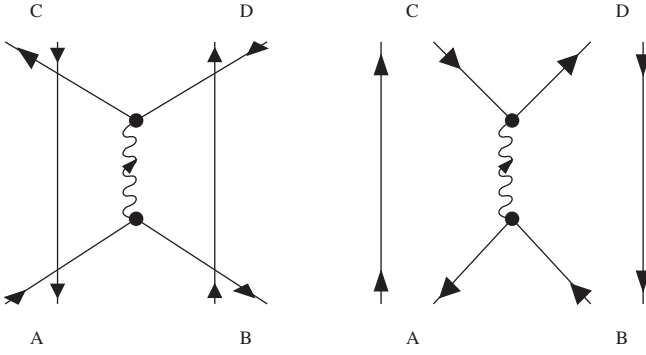


FIG. 1. Left diagram with $q_1 + \bar{q}_2 \rightarrow q_3 + \bar{q}_4$ and right diagram with $\bar{q}_1 + q_2 \rightarrow q_3 + \bar{q}_4$ for $A + B \rightarrow C + D$. The vertical lines represent spectator quarks (antiquarks) of the mesons A, B, C, D .

to the two Feynman diagrams, the S-matrix element for $A + B \rightarrow C + D$ is

$$S_{fi} = \delta_{fi} - 2\pi i \delta(E_f - E_i) (\langle q_3 \bar{q}_1, q_2 \bar{q}_4 | V_{aq_1 \bar{q}_2} | q_1 \bar{q}_1, q_2 \bar{q}_2 \rangle + \langle q_1 \bar{q}_4, q_3 \bar{q}_2 | V_{a\bar{q}_1 q_2} | q_1 \bar{q}_1, q_2 \bar{q}_2 \rangle), \quad (1)$$

where E_i (E_f) is the total energy of the two initial (final) mesons; $V_{aq_1 \bar{q}_2}$ and $V_{a\bar{q}_1 q_2}$ are the transition potentials for $q_1 + \bar{q}_2 \rightarrow q_3 + \bar{q}_4$ and $\bar{q}_1 + q_2 \rightarrow q_3 + \bar{q}_4$, respectively; mesons C and D are individually $q_3 \bar{q}_1$ and $q_2 \bar{q}_2$ in the left diagram and are $q_1 \bar{q}_4$ and $q_3 \bar{q}_2$ in the right diagram. The wave function of the initial mesons is

$$\psi_{q_1 \bar{q}_1, q_2 \bar{q}_2} = \frac{e^{i\vec{P}_{q_1 \bar{q}_1} \cdot \vec{R}_{q_1 \bar{q}_1}}}{\sqrt{V}} \psi_{q_1 \bar{q}_1}(\vec{r}_{q_1 \bar{q}_1}) \frac{e^{i\vec{P}_{q_2 \bar{q}_2} \cdot \vec{R}_{q_2 \bar{q}_2}}}{\sqrt{V}} \psi_{q_2 \bar{q}_2}(\vec{r}_{q_2 \bar{q}_2}), \quad (2)$$

where $\vec{P}_{q_1 \bar{q}_1}$ ($\vec{P}_{q_2 \bar{q}_2}$), $\vec{R}_{q_1 \bar{q}_1}$ ($\vec{R}_{q_2 \bar{q}_2}$), and $\vec{r}_{q_1 \bar{q}_1}$ ($\vec{r}_{q_2 \bar{q}_2}$) are the total momentum, the center-of-mass coordinate, and the relative coordinate of q_1 (q_2) and \bar{q}_1 (\bar{q}_2), respectively. $\psi_{ab}(\vec{r}_{ab})$ is the product of the color wave function, the spin wave function, the flavor wave function, and the relative-motion wave function of constituents a and b . The wave function of the final mesons is

$$\psi_{q_3 \bar{q}_1, q_2 \bar{q}_4} = \frac{e^{i\vec{P}_{q_3 \bar{q}_1} \cdot \vec{R}_{q_3 \bar{q}_1}}}{\sqrt{V}} \psi_{q_3 \bar{q}_1}(\vec{r}_{q_3 \bar{q}_1}) \frac{e^{i\vec{P}_{q_2 \bar{q}_4} \cdot \vec{R}_{q_2 \bar{q}_4}}}{\sqrt{V}} \psi_{q_2 \bar{q}_4}(\vec{r}_{q_2 \bar{q}_4}), \quad (3)$$

corresponding to the left diagram, or

$$\psi_{q_1 \bar{q}_4, q_3 \bar{q}_2} = \frac{e^{i\vec{P}_{q_1 \bar{q}_4} \cdot \vec{R}_{q_1 \bar{q}_4}}}{\sqrt{V}} \psi_{q_1 \bar{q}_4}(\vec{r}_{q_1 \bar{q}_4}) \frac{e^{i\vec{P}_{q_3 \bar{q}_2} \cdot \vec{R}_{q_3 \bar{q}_2}}}{\sqrt{V}} \psi_{q_3 \bar{q}_2}(\vec{r}_{q_3 \bar{q}_2}), \quad (4)$$

corresponding to the right diagram. $\vec{P}_{q_3 \bar{q}_1}$ ($\vec{P}_{q_2 \bar{q}_4}$), $\vec{P}_{q_1 \bar{q}_4}$, $\vec{P}_{q_3 \bar{q}_2}$), $\vec{R}_{q_3 \bar{q}_1}$ ($\vec{R}_{q_2 \bar{q}_4}$), $\vec{R}_{q_1 \bar{q}_4}$, $\vec{R}_{q_3 \bar{q}_2}$), and $\vec{r}_{q_3 \bar{q}_1}$ ($\vec{r}_{q_2 \bar{q}_4}$), $\vec{r}_{q_1 \bar{q}_4}$, $\vec{r}_{q_3 \bar{q}_2}$) are the total momentum, the center-of-mass coordinate, and the relative coordinate of q_3 and \bar{q}_1 (q_2 and \bar{q}_4 , q_1 and \bar{q}_4 , q_3 and \bar{q}_2), respectively. Every meson wave function is normalized in the volume V .

We first deal with

$$\begin{aligned} & \langle q_3 \bar{q}_1, q_2 \bar{q}_4 | V_{aq_1 \bar{q}_2} | q_1 \bar{q}_1, q_2 \bar{q}_2 \rangle \\ &= \int d\vec{r}_{q_1} d\vec{r}_{\bar{q}_1} d\vec{r}_{q_2} d\vec{r}_{\bar{q}_2} \frac{e^{-i\vec{P}_{q_3 \bar{q}_1} \cdot \vec{R}_{q_3 \bar{q}_1}}}{\sqrt{V}} \psi_{q_3 \bar{q}_1}^+(\vec{r}_{q_3 \bar{q}_1}) \\ &\quad \times \frac{e^{-i\vec{P}_{q_2 \bar{q}_4} \cdot \vec{R}_{q_2 \bar{q}_4}}}{\sqrt{V}} \psi_{q_2 \bar{q}_4}^+(\vec{r}_{q_2 \bar{q}_4}) V_{aq_1 \bar{q}_2} \frac{e^{i\vec{P}_{q_1 \bar{q}_1} \cdot \vec{R}_{q_1 \bar{q}_1}}}{\sqrt{V}} \psi_{q_1 \bar{q}_1}(\vec{r}_{q_1 \bar{q}_1}) \\ &\quad \times \frac{e^{i\vec{P}_{q_2 \bar{q}_2} \cdot \vec{R}_{q_2 \bar{q}_2}}}{\sqrt{V}} \psi_{q_2 \bar{q}_2}(\vec{r}_{q_2 \bar{q}_2}). \end{aligned} \quad (5)$$

Let \vec{R}_{total} be the center-of-mass coordinate of the two initial or final mesons, \vec{P}_i (\vec{P}_f) the total three-dimensional momentum of the two initial (final) mesons, and $m_{q_1 \bar{q}_1}$ ($m_{q_2 \bar{q}_2}$, $m_{q_3 \bar{q}_1}$, $m_{q_2 \bar{q}_4}$, $m_{q_1 \bar{q}_4}$, $m_{q_3 \bar{q}_2}$) the mass of $q_1 \bar{q}_1$ ($q_2 \bar{q}_2$, $q_3 \bar{q}_1$, $q_2 \bar{q}_4$, $q_1 \bar{q}_4$, $q_3 \bar{q}_2$). Denote the relative coordinate and the relative momentum of $q_1 \bar{q}_1$ and $q_2 \bar{q}_2$ by $\vec{r}_{q_1 \bar{q}_1, q_2 \bar{q}_2}$ and $\vec{p}_{q_1 \bar{q}_1, q_2 \bar{q}_2}$, respectively. We have

$$\vec{R}_{q_1 \bar{q}_1} = \vec{R}_{\text{total}} + \frac{m_{q_2 \bar{q}_2}}{m_{q_1 \bar{q}_1} + m_{q_2 \bar{q}_2}} \vec{r}_{q_1 \bar{q}_1, q_2 \bar{q}_2}, \quad (6)$$

$$\vec{R}_{q_2 \bar{q}_2} = \vec{R}_{\text{total}} - \frac{m_{q_1 \bar{q}_1}}{m_{q_1 \bar{q}_1} + m_{q_2 \bar{q}_2}} \vec{r}_{q_1 \bar{q}_1, q_2 \bar{q}_2}, \quad (7)$$

$$\vec{P}_{q_1 \bar{q}_1} = \frac{m_{q_1 \bar{q}_1}}{m_{q_1 \bar{q}_1} + m_{q_2 \bar{q}_2}} \vec{P}_i + \vec{p}_{q_1 \bar{q}_1, q_2 \bar{q}_2}, \quad (8)$$

$$\vec{P}_{q_2 \bar{q}_2} = \frac{m_{q_2 \bar{q}_2}}{m_{q_1 \bar{q}_1} + m_{q_2 \bar{q}_2}} \vec{P}_i - \vec{p}_{q_1 \bar{q}_1, q_2 \bar{q}_2}. \quad (9)$$

Denote the relative coordinate and the relative momentum of $q_3 \bar{q}_1$ and $q_2 \bar{q}_4$ by $\vec{r}_{q_3 \bar{q}_1, q_2 \bar{q}_4}$ and $\vec{p}_{q_3 \bar{q}_1, q_2 \bar{q}_4}$, respectively. We have

$$\vec{R}_{q_3 \bar{q}_1} = \vec{R}_{\text{total}} + \frac{m_{q_2 \bar{q}_4}}{m_{q_3 \bar{q}_1} + m_{q_2 \bar{q}_4}} \vec{r}_{q_3 \bar{q}_1, q_2 \bar{q}_4}, \quad (10)$$

$$\vec{R}_{q_2 \bar{q}_4} = \vec{R}_{\text{total}} - \frac{m_{q_3 \bar{q}_1}}{m_{q_3 \bar{q}_1} + m_{q_2 \bar{q}_4}} \vec{r}_{q_3 \bar{q}_1, q_2 \bar{q}_4}, \quad (11)$$

$$\vec{P}_{q_3 \bar{q}_1} = \frac{m_{q_3 \bar{q}_1}}{m_{q_3 \bar{q}_1} + m_{q_2 \bar{q}_4}} \vec{P}_f + \vec{p}_{q_3 \bar{q}_1, q_2 \bar{q}_4}, \quad (12)$$

$$\vec{P}_{q_2 \bar{q}_4} = \frac{m_{q_2 \bar{q}_4}}{m_{q_3 \bar{q}_1} + m_{q_2 \bar{q}_4}} \vec{P}_f - \vec{p}_{q_3 \bar{q}_1, q_2 \bar{q}_4}. \quad (13)$$

From Eqs. (6), (7), (10), and (11) we obtain

$$\begin{aligned}\vec{r}_{q_1} &= \vec{r}_{q_1\bar{q}_1} + \frac{m_{q_2}m_{q_3}}{m_{\bar{q}_1}(m_{q_2} + m_{\bar{q}_4})} \vec{r}_{q_2\bar{q}_4} \\ &\quad + \frac{m_{q_3} + m_{\bar{q}_1}}{m_{\bar{q}_1}} \vec{R}_{q_3\bar{q}_1} - \frac{m_{q_3}}{m_{\bar{q}_1}} \vec{R}_{q_2\bar{q}_4},\end{aligned}\quad (14)$$

$$\vec{r}_{\bar{q}_1} = \frac{m_{q_2}m_{q_3}}{m_{\bar{q}_1}(m_{q_2} + m_{\bar{q}_4})} \vec{r}_{q_2\bar{q}_4} + \frac{m_{q_3} + m_{\bar{q}_1}}{m_{\bar{q}_1}} \vec{R}_{q_3\bar{q}_1} - \frac{m_{q_3}}{m_{\bar{q}_1}} \vec{R}_{q_2\bar{q}_4},\quad (15)$$

$$\vec{r}_{q_2} = \frac{m_{\bar{q}_4}}{m_{q_2} + m_{\bar{q}_4}} \vec{r}_{q_2\bar{q}_4} + \vec{R}_{q_2\bar{q}_4},\quad (16)$$

which lead to

$$\begin{aligned}d\vec{r}_{q_1} d\vec{r}_{\bar{q}_1} d\vec{r}_{q_2} d\vec{r}_{q_3} &= \frac{(m_{q_3} + m_{\bar{q}_1})^3}{m_{\bar{q}_1}^3} d\vec{r}_{q_1\bar{q}_1} d\vec{r}_{q_2\bar{q}_4} d\vec{R}_{q_3\bar{q}_1} d\vec{R}_{q_2\bar{q}_4} \\ &= \frac{(m_{q_3} + m_{\bar{q}_1})^3}{m_{\bar{q}_1}^3} \\ &\quad \times d\vec{r}_{q_1\bar{q}_1} d\vec{r}_{q_2\bar{q}_4} d\vec{r}_{q_3\bar{q}_1, q_2\bar{q}_4} d\vec{R}_{\text{total}},\end{aligned}\quad (18)$$

where constituent a has the mass m_a and the position vector \vec{r}_a . Equation (5) becomes

$$\begin{aligned}\langle q_3\bar{q}_1, q_2\bar{q}_4 | V_{a\bar{q}_1\bar{q}_2} | q_1\bar{q}_1, q_2\bar{q}_2 \rangle &= \frac{(m_{q_3} + m_{\bar{q}_1})^3}{m_{\bar{q}_1}^3} \int d\vec{r}_{q_1\bar{q}_1} d\vec{r}_{q_2\bar{q}_4} d\vec{r}_{q_3\bar{q}_1, q_2\bar{q}_4} d\vec{R}_{\text{total}} \\ &\quad \times \frac{\psi_{q_3\bar{q}_1}^+(\vec{r}_{q_3\bar{q}_1}) \psi_{q_2\bar{q}_4}^+(\vec{r}_{q_2\bar{q}_4})}{\sqrt{V}} e^{-i\vec{P}_f \cdot \vec{R}_{\text{total}} - i\vec{p}_{q_3\bar{q}_1, q_2\bar{q}_4} \cdot \vec{r}_{q_3\bar{q}_1, q_2\bar{q}_4}} V_{a\bar{q}_1\bar{q}_2} \frac{\psi_{q_1\bar{q}_1}(\vec{r}_{q_1\bar{q}_1}) \psi_{q_2\bar{q}_2}(\vec{r}_{q_2\bar{q}_2})}{\sqrt{V}} e^{i\vec{P}_i \cdot \vec{R}_{\text{total}} + i\vec{p}_{q_1\bar{q}_1, q_2\bar{q}_2} \cdot \vec{r}_{q_1\bar{q}_1, q_2\bar{q}_2}} \\ &= \frac{(m_{q_3} + m_{\bar{q}_1})^3}{m_{\bar{q}_1}^3} (2\pi)^3 \delta(\vec{P}_f - \vec{P}_i) \int d\vec{r}_{q_1\bar{q}_1} d\vec{r}_{q_2\bar{q}_4} d\vec{r}_{q_3\bar{q}_1, q_2\bar{q}_4} \frac{\psi_{q_3\bar{q}_1}^+(\vec{r}_{q_3\bar{q}_1}) \psi_{q_2\bar{q}_4}^+(\vec{r}_{q_2\bar{q}_4})}{\sqrt{V}} V_{a\bar{q}_1\bar{q}_2} \\ &\quad \times \frac{\psi_{q_1\bar{q}_1}(\vec{r}_{q_1\bar{q}_1}) \psi_{q_2\bar{q}_2}(\vec{r}_{q_2\bar{q}_2})}{\sqrt{V}} e^{i\vec{p}_{q_1\bar{q}_1, q_2\bar{q}_2} \cdot \vec{r}_{q_1\bar{q}_1, q_2\bar{q}_2} - i\vec{p}_{q_3\bar{q}_1, q_2\bar{q}_4} \cdot \vec{r}_{q_3\bar{q}_1, q_2\bar{q}_4}} \\ &= (2\pi)^3 \delta(\vec{P}_f - \vec{P}_i) \frac{\mathcal{M}_{a\bar{q}_1\bar{q}_2}}{V^2 \sqrt{2E_A 2E_B 2E_C 2E_D}},\end{aligned}\quad (19)$$

where E_A (E_B, E_C, E_D) is the energy of meson A (B, C, D), and

$$\begin{aligned}\mathcal{M}_{a\bar{q}_1\bar{q}_2} &= \frac{(m_{q_3} + m_{\bar{q}_1})^3}{m_{\bar{q}_1}^3} \sqrt{2E_A 2E_B 2E_C 2E_D} \\ &\quad \times \int d\vec{r}_{q_1\bar{q}_1} d\vec{r}_{q_2\bar{q}_4} d\vec{r}_{q_3\bar{q}_1, q_2\bar{q}_4} \psi_{q_3\bar{q}_1}^+(\vec{r}_{q_3\bar{q}_1}) \\ &\quad \times \psi_{q_2\bar{q}_4}^+(\vec{r}_{q_2\bar{q}_4}) V_{a\bar{q}_1\bar{q}_2} \psi_{q_1\bar{q}_1}(\vec{r}_{q_1\bar{q}_1}) \psi_{q_2\bar{q}_2}(\vec{r}_{q_2\bar{q}_2}) \\ &\quad \times e^{i\vec{p}_{q_1\bar{q}_1, q_2\bar{q}_2} \cdot \vec{r}_{q_1\bar{q}_1, q_2\bar{q}_2} - i\vec{p}_{q_3\bar{q}_1, q_2\bar{q}_4} \cdot \vec{r}_{q_3\bar{q}_1, q_2\bar{q}_4}}.\end{aligned}\quad (20)$$

We now address

$$\begin{aligned}\langle q_1\bar{q}_4, q_3\bar{q}_2 | V_{a\bar{q}_1\bar{q}_2} | q_1\bar{q}_1, q_2\bar{q}_2 \rangle &= \int d\vec{r}_{q_1} d\vec{r}_{q_2} d\vec{r}_{\bar{q}_2} d\vec{r}_{q_3} \frac{e^{-i\vec{P}_{q_1\bar{q}_4} \cdot \vec{R}_{q_1\bar{q}_4}}}{\sqrt{V}} \psi_{q_1\bar{q}_4}^+(\vec{r}_{q_1\bar{q}_4}) \\ &\quad \times \frac{e^{-i\vec{P}_{q_3\bar{q}_2} \cdot \vec{R}_{q_3\bar{q}_2}}}{\sqrt{V}} \psi_{q_3\bar{q}_2}^+(\vec{r}_{q_3\bar{q}_2}) V_{a\bar{q}_1\bar{q}_2} \\ &\quad \times \frac{e^{i\vec{p}_{q_1\bar{q}_1} \cdot \vec{R}_{q_1\bar{q}_1}}}{\sqrt{V}} \psi_{q_1\bar{q}_1}(\vec{r}_{q_1\bar{q}_1}) \frac{e^{i\vec{p}_{q_2\bar{q}_2} \cdot \vec{R}_{q_2\bar{q}_2}}}{\sqrt{V}} \psi_{q_2\bar{q}_2}(\vec{r}_{q_2\bar{q}_2}).\end{aligned}\quad (21)$$

Let us denote the relative coordinate and the relative momentum of $q_1\bar{q}_4$ and $q_3\bar{q}_2$ by $\vec{r}_{q_1\bar{q}_4, q_3\bar{q}_2}$ and $\vec{p}_{q_1\bar{q}_4, q_3\bar{q}_2}$, respectively. We have

$$\vec{R}_{q_1\bar{q}_4} = \vec{R}_{\text{total}} + \frac{m_{q_3\bar{q}_2}}{m_{q_1\bar{q}_4} + m_{q_3\bar{q}_2}} \vec{r}_{q_1\bar{q}_4, q_3\bar{q}_2},\quad (22)$$

$$\vec{R}_{q_3\bar{q}_2} = \vec{R}_{\text{total}} - \frac{m_{q_1\bar{q}_4}}{m_{q_1\bar{q}_4} + m_{q_3\bar{q}_2}} \vec{r}_{q_1\bar{q}_4, q_3\bar{q}_2},\quad (23)$$

$$\vec{P}_{q_1\bar{q}_4} = \frac{m_{q_1\bar{q}_4}}{m_{q_1\bar{q}_4} + m_{q_3\bar{q}_2}} \vec{P}_f + \vec{p}_{q_1\bar{q}_4, q_3\bar{q}_2},\quad (24)$$

$$\vec{P}_{q_3\bar{q}_2} = \frac{m_{q_3\bar{q}_2}}{m_{q_1\bar{q}_4} + m_{q_3\bar{q}_2}} \vec{P}_f - \vec{p}_{q_1\bar{q}_4, q_3\bar{q}_2}.\quad (25)$$

From Eqs. (6), (7), (22), and (23) we obtain

$$\begin{aligned}\vec{r}_{q_1} &= -\frac{m_{\bar{q}_2}m_{\bar{q}_4}}{m_{q_1}(m_{q_3} + m_{\bar{q}_2})} \vec{r}_{q_3\bar{q}_2} + \frac{m_{q_1} + m_{\bar{q}_4}}{m_{q_1}} \vec{R}_{q_1\bar{q}_4} \\ &\quad - \frac{m_{\bar{q}_4}}{m_{\bar{q}_1}} \vec{R}_{q_3\bar{q}_2},\end{aligned}\quad (26)$$

$$\vec{r}_{q_2} = -\vec{r}_{q_1\bar{q}_1} - \frac{m_{\bar{q}_2} m_{\bar{q}_4}}{m_{q_1}(m_{q_3} + m_{\bar{q}_2})} \vec{r}_{q_3\bar{q}_2} + \frac{m_{q_1} + m_{\bar{q}_4}}{m_{q_1}} \vec{R}_{q_1\bar{q}_4} \\ - \frac{m_{\bar{q}_4}}{m_{q_1}} \vec{R}_{q_3\bar{q}_2}, \quad (27)$$

$$\vec{r}_{\bar{q}_2} = -\frac{m_{q_3}}{m_{q_3} + m_{\bar{q}_2}} \vec{r}_{q_3\bar{q}_2} + \vec{R}_{q_3\bar{q}_2}, \quad (28)$$

$$\vec{r}_{q_3} = \frac{m_{\bar{q}_2}}{m_{q_3} + m_{\bar{q}_2}} \vec{r}_{q_3\bar{q}_2} + \vec{R}_{q_3\bar{q}_2}, \quad (29)$$

which lead to

$$d\vec{r}_{q_1} d\vec{r}_{q_2} d\vec{r}_{\bar{q}_2} d\vec{r}_{q_3} = \frac{(m_{q_1} + m_{\bar{q}_4})^3}{m_{q_1}^3} d\vec{r}_{q_1\bar{q}_1} d\vec{r}_{q_3\bar{q}_2} d\vec{R}_{q_1\bar{q}_4} d\vec{R}_{q_3\bar{q}_2} \\ = \frac{(m_{q_1} + m_{\bar{q}_4})^3}{m_{q_1}^3} \\ \times d\vec{r}_{q_1\bar{q}_1} d\vec{r}_{q_3\bar{q}_2} d\vec{r}_{q_1\bar{q}_4, q_3\bar{q}_2} d\vec{R}_{\text{total}}. \quad (30)$$

Then Eq. (21) becomes

$$\langle q_1\bar{q}_4, q_3\bar{q}_2 | V_{a\bar{q}_1q_2} | q_1\bar{q}_1, q_2\bar{q}_2 \rangle = \frac{(m_{q_1} + m_{\bar{q}_4})^3}{m_{q_1}^3} \int d\vec{r}_{q_1\bar{q}_1} d\vec{r}_{q_3\bar{q}_2} d\vec{r}_{q_1\bar{q}_4, q_3\bar{q}_2} d\vec{R}_{\text{total}} \frac{\psi_{q_1\bar{q}_4}^+(\vec{r}_{q_1\bar{q}_4})}{\sqrt{V}} \frac{\psi_{q_3\bar{q}_2}^+(\vec{r}_{q_3\bar{q}_2})}{\sqrt{V}} \\ \times e^{-i\vec{P}_f \cdot \vec{R}_{\text{total}} - i\vec{p}_{q_1\bar{q}_4, q_3\bar{q}_2} \cdot \vec{r}_{q_1\bar{q}_4, q_3\bar{q}_2}} V_{a\bar{q}_1q_2} \frac{\psi_{q_1\bar{q}_1}(\vec{r}_{q_1\bar{q}_1})}{\sqrt{V}} \frac{\psi_{q_2\bar{q}_2}(\vec{r}_{q_2\bar{q}_2})}{\sqrt{V}} e^{i\vec{P}_i \cdot \vec{R}_{\text{total}} + i\vec{p}_{q_1\bar{q}_1, q_2\bar{q}_2} \cdot \vec{r}_{q_1\bar{q}_1, q_2\bar{q}_2}} \\ = \frac{(m_{q_1} + m_{\bar{q}_4})^3}{m_{q_1}^3} (2\pi)^3 \delta(\vec{P}_f - \vec{P}_i) \int d\vec{r}_{q_1\bar{q}_1} d\vec{r}_{q_3\bar{q}_2} d\vec{r}_{q_1\bar{q}_4, q_3\bar{q}_2} \frac{\psi_{q_1\bar{q}_4}^+(\vec{r}_{q_1\bar{q}_4})}{\sqrt{V}} \frac{\psi_{q_3\bar{q}_2}^+(\vec{r}_{q_3\bar{q}_2})}{\sqrt{V}} \\ \times V_{a\bar{q}_1q_2} \frac{\psi_{q_1\bar{q}_1}(\vec{r}_{q_1\bar{q}_1})}{\sqrt{V}} \frac{\psi_{q_2\bar{q}_2}(\vec{r}_{q_2\bar{q}_2})}{\sqrt{V}} e^{i\vec{p}_{q_1\bar{q}_1, q_2\bar{q}_2} \cdot \vec{r}_{q_1\bar{q}_1, q_2\bar{q}_2} - i\vec{p}_{q_1\bar{q}_4, q_3\bar{q}_2} \cdot \vec{r}_{q_1\bar{q}_4, q_3\bar{q}_2}} \\ = (2\pi)^3 \delta(\vec{P}_f - \vec{P}_i) \frac{\mathcal{M}_{a\bar{q}_1q_2}}{V^2 \sqrt{2E_A 2E_B 2E_C 2E_D}}, \quad (31)$$

where

$$\mathcal{M}_{a\bar{q}_1q_2} = \frac{(m_{q_1} + m_{\bar{q}_4})^3}{m_{q_1}^3} \sqrt{2E_A 2E_B 2E_C 2E_D} \\ \times \int d\vec{r}_{q_1\bar{q}_1} d\vec{r}_{q_3\bar{q}_2} d\vec{r}_{q_1\bar{q}_4, q_3\bar{q}_2} \\ \times \psi_{q_1\bar{q}_4}^+(\vec{r}_{q_1\bar{q}_4}) \psi_{q_3\bar{q}_2}^+(\vec{r}_{q_3\bar{q}_2}) V_{a\bar{q}_1q_2} \\ \times \psi_{q_1\bar{q}_1}(\vec{r}_{q_1\bar{q}_1}) \psi_{q_2\bar{q}_2}(\vec{r}_{q_2\bar{q}_2}) \\ \times e^{i\vec{p}_{q_1\bar{q}_1, q_2\bar{q}_2} \cdot \vec{r}_{q_1\bar{q}_1, q_2\bar{q}_2} - i\vec{p}_{q_1\bar{q}_4, q_3\bar{q}_2} \cdot \vec{r}_{q_1\bar{q}_4, q_3\bar{q}_2}}. \quad (32)$$

Meson i ($i = A, B, C, D$) has the mass m_i , the four-momentum $P_i = (E_i, \vec{P}_i)$, and the angular momentum J_i with its magnetic projection quantum number J_{iz} . The unpolarized cross section for $A + B \rightarrow C + D$ is

$$\sigma^{\text{unpol}}(\sqrt{s}, T) = \frac{(2\pi)^4}{4\sqrt{(P_A \cdot P_B)^2 - m_A^2 m_B^2}} \\ \times \int \frac{d^3 P_C}{(2\pi)^3 2E_C} \frac{d^3 P_D}{(2\pi)^3 2E_D} \frac{1}{(2J_A + 1)(2J_B + 1)} \\ \times \sum_{J_{Az} J_{Bz} J_{Cz} J_{Dz}} |\mathcal{M}_{a\bar{q}_1\bar{q}_2} + \mathcal{M}_{a\bar{q}_1q_2}|^2 \delta(E_f - E_i) \delta(\vec{P}_f - \vec{P}_i), \quad (33)$$

where s is the Mandelstam variable given by $s = (E_A + E_B)^2 - (\vec{P}_A + \vec{P}_B)^2$, and T is the temperature. In the center-of-mass frame of A and B the three-dimensional momenta of mesons A and C are \vec{P} and \vec{P}' , respectively. Denote the angle between \vec{P} and \vec{P}' by θ . The unpolarized cross section is given by

$$\sigma^{\text{unpol}}(\sqrt{s}, T) = \frac{1}{(2J_A + 1)(2J_B + 1)} \frac{1}{32\pi s} \frac{|\vec{P}'(\sqrt{s})|}{|\vec{P}(\sqrt{s})|} \\ \times \int_0^\pi d\theta \sum_{J_{Az} J_{Bz} J_{Cz} J_{Dz}} |\mathcal{M}_{a\bar{q}_1\bar{q}_2} + \mathcal{M}_{a\bar{q}_1q_2}|^2 \sin\theta. \quad (34)$$

III. TRANSITION POTENTIAL

In the reaction $A + B \rightarrow C + D$ the quark of an initial meson annihilates with the antiquark of another meson to produce a gluon, and subsequently this gluon creates a quark to form a final meson and an antiquark to form another final meson. The quark-antiquark annihilation and creation, $q(p_1) + \bar{q}(-p_2) \rightarrow q'(p_3) + \bar{q}'(-p_4)$, is shown in Fig. 2. The initial quark wave function is

$$\psi_q(\vec{p}_1, s_{qz}) = \begin{pmatrix} G_1(\vec{p}_1) \\ \frac{\vec{G}_1 \cdot \vec{p}_1}{2m_q} G_1(\vec{p}_1) \end{pmatrix} \chi_{s_{qz}}, \quad (35)$$

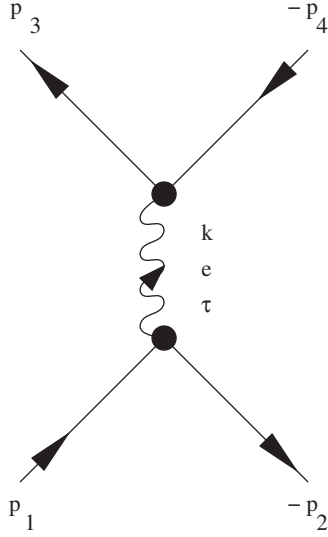


FIG. 2. Quark-antiquark annihilation and creation: $q(p_1) + \bar{q}(-p_2) \rightarrow q'(p_3) + \bar{q}'(-p_4)$, where k denotes the gluon four-momentum, e its color index, and τ its space-time index [cf. Eq. (39)].

and the final quark wave function is

$$\psi_{q'}(\vec{p}_3, s_{q'z}) = \left(\frac{G_3(\vec{p}_3)}{\frac{\vec{\sigma} \cdot \vec{p}_3}{2m_{q'}} G_3(\vec{p}_3)} \right) \chi_{s_{q'z}}, \quad (36)$$

where $\vec{\sigma}$ are the Pauli matrices; $\chi_{s_{qz}}$ and $\chi_{s_{q'z}}$ are the spin wave functions with the magnetic projection quantum

numbers, s_{qz} and $s_{q'z}$, of the quark spin, respectively. The initial antiquark wave function is

$$\psi_{\bar{q}}(\vec{p}_2, s_{\bar{q}z}) = \left(\frac{\frac{\vec{\sigma} \cdot \vec{p}_2}{2m_{\bar{q}}} G_2(\vec{p}_2)}{G_2(\vec{p}_2)} \right) \chi_{s_{\bar{q}z}}, \quad (37)$$

and the final antiquark wave function is

$$\psi_{\bar{q}'}(\vec{p}_4, s_{\bar{q}'z}) = \left(\frac{\frac{\vec{\sigma} \cdot \vec{p}_4}{2m_{\bar{q}'}} G_4(\vec{p}_4)}{G_4(\vec{p}_4)} \right) \chi_{s_{\bar{q}'z}}, \quad (38)$$

where $m_{\bar{q}} = m_q$, $m_{\bar{q}'} = m_{q'}$, and $\chi_{s_{\bar{q}z}}$ and $\chi_{s_{\bar{q}'z}}$ are the spin wave functions with the magnetic projection quantum numbers, $s_{\bar{q}z}$ and $s_{\bar{q}'z}$, of the antiquark spin, respectively. In Eqs. (35)–(38) the color and flavor wave functions are suppressed. According to the Feynman rules given in Ref. [13], the amplitude for the Feynman diagram in Fig. 2 is written as

$$\begin{aligned} \mathcal{M}_a = & \frac{g_s^2}{k^2} \bar{\psi}_{q'}(\vec{p}_3, s_{q'z}) \gamma_\tau T^e \psi_{\bar{q}}(\vec{p}_4, s_{\bar{q}z}) \\ & \times \bar{\psi}_{\bar{q}}(\vec{p}_2, s_{\bar{q}z}) \gamma^\tau T^e \psi_q(\vec{p}_1, s_{qz}), \end{aligned} \quad (39)$$

where g_s is the gauge coupling constant, T^e ($e = 1, \dots, 8$) are the $SU(3)$ color generators, and $T^e T^e = \frac{\vec{\lambda}(34)}{2} \cdot \frac{\vec{\lambda}(21)}{2}$ with $\vec{\lambda}$ the Gell-Mann matrices. Repeated color and space-time indices (τ) are summed. Using these quark and antiquark wave functions, the amplitude to order of the inverse of the (constituent) quark mass squared is

$$\begin{aligned} \mathcal{M}_a = & \frac{g_s^2}{k^2} \left[\chi_{s_{q'z}}^+ \chi_{s_{\bar{q}z}}^+ T_e T_e G_3(\vec{p}_3) G_2(\vec{p}_2) \frac{\vec{\sigma}(34) \cdot \vec{k} \vec{\sigma}(21) \cdot \vec{k}}{4m_{q'} m_q} G_4(\vec{p}_4) G_1(\vec{p}_1) \chi_{s_{\bar{q}'z}} \chi_{s_{qz}} \right. \\ & - \chi_{s_{q'z}}^+ \chi_{s_{\bar{q}z}}^+ T_e T_e G_3(\vec{p}_3) G_2(\vec{p}_2) \left(\vec{\sigma}(34) \cdot \vec{\sigma}(21) + \frac{\vec{\sigma}(21) \cdot \vec{p}_2 \vec{\sigma}(34) \cdot \vec{\sigma}(21) \vec{\sigma}(21) \cdot \vec{p}_1}{4m_q^2} \right. \\ & \left. \left. + \frac{\vec{\sigma}(34) \cdot \vec{p}_3 \vec{\sigma}(34) \cdot \vec{\sigma}(21) \vec{\sigma}(34) \cdot \vec{p}_4}{4m_{q'}^2} \right) G_4(\vec{p}_4) G_1(\vec{p}_1) \chi_{s_{\bar{q}'z}} \chi_{s_{qz}} \right]. \end{aligned} \quad (40)$$

From the expression of the amplitude we obtain the transition potential for $q(p_1) + \bar{q}(-p_2) \rightarrow q'(p_3) + \bar{q}'(-p_4)$,

$$\begin{aligned} V_{aq\bar{q}}(\vec{k}) = & \frac{g_s^2 \vec{\lambda}(34) \cdot \vec{\lambda}(21)}{k^2} \left(\frac{\vec{\sigma}(34) \cdot \vec{k} \vec{\sigma}(21) \cdot \vec{k}}{4m_{q'} m_q} - \vec{\sigma}(34) \cdot \vec{\sigma}(21) \right. \\ & \left. - \frac{\vec{\sigma}(21) \cdot \vec{p}_2 \vec{\sigma}(34) \cdot \vec{\sigma}(21) \vec{\sigma}(21) \cdot \vec{p}_1}{4m_q^2} \right. \\ & \left. - \frac{\vec{\sigma}(34) \cdot \vec{p}_3 \vec{\sigma}(34) \cdot \vec{\sigma}(21) \vec{\sigma}(34) \cdot \vec{p}_4}{4m_{q'}^2} \right), \end{aligned} \quad (41)$$

where $\vec{\lambda}(34)$ [$\vec{\lambda}(21)$] mean that they have matrix elements between the color wave functions of the final (initial) quark and the final (initial) antiquark, and $\vec{\sigma}(34)$ [$\vec{\sigma}(21)$] mean that they have matrix elements between the spin wave functions of the final (initial) quark and the final (initial) antiquark.

IV. TRANSITION AMPLITUDE

In order to obtain the unpolarized cross section, we calculate the transition amplitudes, $\mathcal{M}_{aq_1\bar{q}_2}$ and $\mathcal{M}_{a\bar{q}_1q_2}$. We take the Fourier transform of the meson wave functions, $V_{aq_1\bar{q}_2}$ in Eq. (20), and $V_{a\bar{q}_1q_2}$ in Eq. (32):

$$\psi_{q_1\bar{q}_1}(\vec{r}_{q_1\bar{q}_1}) = \int \frac{d^3 p_{q_1\bar{q}_1}}{(2\pi)^3} \psi_{q_1\bar{q}_1}(\vec{p}_{q_1\bar{q}_1}) e^{i\vec{p}_{q_1\bar{q}_1}\cdot\vec{r}_{q_1\bar{q}_1}}, \quad (42)$$

$$\psi_{q_2\bar{q}_2}(\vec{r}_{q_2\bar{q}_2}) = \int \frac{d^3 p_{q_2\bar{q}_2}}{(2\pi)^3} \psi_{q_2\bar{q}_2}(\vec{p}_{q_2\bar{q}_2}) e^{i\vec{p}_{q_2\bar{q}_2}\cdot\vec{r}_{q_2\bar{q}_2}}, \quad (43)$$

$$\psi_{q_3\bar{q}_1}(\vec{r}_{q_3\bar{q}_1}) = \int \frac{d^3 p_{q_3\bar{q}_1}}{(2\pi)^3} \psi_{q_3\bar{q}_1}(\vec{p}_{q_3\bar{q}_1}) e^{i\vec{p}_{q_3\bar{q}_1}\cdot\vec{r}_{q_3\bar{q}_1}}, \quad (44)$$

$$\psi_{q_2\bar{q}_4}(\vec{r}_{q_2\bar{q}_4}) = \int \frac{d^3 p_{q_2\bar{q}_4}}{(2\pi)^3} \psi_{q_2\bar{q}_4}(\vec{p}_{q_2\bar{q}_4}) e^{i\vec{p}_{q_2\bar{q}_4}\cdot\vec{r}_{q_2\bar{q}_4}}, \quad (45)$$

$$\psi_{q_1\bar{q}_4}(\vec{r}_{q_1\bar{q}_4}) = \int \frac{d^3 p_{q_1\bar{q}_4}}{(2\pi)^3} \psi_{q_1\bar{q}_4}(\vec{p}_{q_1\bar{q}_4}) e^{i\vec{p}_{q_1\bar{q}_4}\cdot\vec{r}_{q_1\bar{q}_4}}, \quad (46)$$

$$\psi_{q_3\bar{q}_2}(\vec{r}_{q_3\bar{q}_2}) = \int \frac{d^3 p_{q_3\bar{q}_2}}{(2\pi)^3} \psi_{q_3\bar{q}_2}(\vec{p}_{q_3\bar{q}_2}) e^{i\vec{p}_{q_3\bar{q}_2}\cdot\vec{r}_{q_3\bar{q}_2}}, \quad (47)$$

$$V_{a\bar{q}_1\bar{q}_2}(\vec{r}_{q_3} - \vec{r}_{q_1}) = \int \frac{d^3 k}{(2\pi)^3} V_{a\bar{q}_1\bar{q}_2}(\vec{k}) e^{i\vec{k}\cdot(\vec{r}_{q_3} - \vec{r}_{q_1})}, \quad (48)$$

$$V_{a\bar{q}_1\bar{q}_2}(\vec{r}_{q_3} - \vec{r}_{q_2}) = \int \frac{d^3 k}{(2\pi)^3} V_{a\bar{q}_1\bar{q}_2}(\vec{k}) e^{i\vec{k}\cdot(\vec{r}_{q_3} - \vec{r}_{q_2})}, \quad (49)$$

where \vec{p}_{ab} is the relative momentum of constituents a and b . The transition amplitudes are then calculated in momentum space by the following expressions:

$$\begin{aligned} \mathcal{M}_{a\bar{q}_1\bar{q}_2} &= \sqrt{2E_A 2E_B 2E_C 2E_D} \int \frac{d^3 p_{q_1\bar{q}_1}}{(2\pi)^3} \frac{d^3 p_{q_2\bar{q}_2}}{(2\pi)^3} \\ &\times \psi_{q_3\bar{q}_1}^+(\vec{p}_{q_3\bar{q}_1}) \psi_{q_2\bar{q}_4}^+(\vec{p}_{q_2\bar{q}_4}) V_{a\bar{q}_1\bar{q}_2}(\vec{k}) \\ &\times \psi_{q_1\bar{q}_1}(\vec{p}_{q_1\bar{q}_1}) \psi_{q_2\bar{q}_2}(\vec{p}_{q_2\bar{q}_2}), \end{aligned} \quad (50)$$

$$\begin{aligned} \mathcal{M}_{a\bar{q}_1\bar{q}_2} &= \sqrt{2E_A 2E_B 2E_C 2E_D} \int \frac{d^3 p_{q_1\bar{q}_1}}{(2\pi)^3} \frac{d^3 p_{q_2\bar{q}_2}}{(2\pi)^3} \\ &\times \psi_{q_1\bar{q}_4}^+(\vec{p}_{q_1\bar{q}_4}) \psi_{q_3\bar{q}_2}^+(\vec{p}_{q_3\bar{q}_2}) V_{a\bar{q}_1\bar{q}_2}(\vec{k}) \\ &\times \psi_{q_1\bar{q}_1}(\vec{p}_{q_1\bar{q}_1}) \psi_{q_2\bar{q}_2}(\vec{p}_{q_2\bar{q}_2}). \end{aligned} \quad (51)$$

For convenience sake we also use the notation ψ_A , ψ_B , ψ_C , and ψ_D : $\psi_A = \psi_{q_1\bar{q}_1}$, $\psi_B = \psi_{q_2\bar{q}_2}$, $\psi_C = \psi_{q_3\bar{q}_1} = \psi_{q_1\bar{q}_4}$, and $\psi_D = \psi_{q_2\bar{q}_4} = \psi_{q_3\bar{q}_2}$. The wave functions of mesons A , B , C , and D are individually given by

$$\psi_A = \phi_{A\text{ rel}} \phi_{A\text{ color}} \phi_{A\text{ flavor}} \chi_{S_A S_{A_z}}, \quad (52)$$

$$\psi_B = \phi_{B\text{ rel}} \phi_{B\text{ color}} \phi_{B\text{ flavor}} \chi_{S_B S_{B_z}}, \quad (53)$$

$$\psi_C = \phi_{C\text{ rel}} \phi_{C\text{ color}} \phi_{C\text{ flavor}} \chi_{S_C S_{C_z}}, \quad (54)$$

where $\phi_{A\text{ rel}}$ ($\phi_{B\text{ rel}}$, $\phi_{C\text{ rel}}$, $\phi_{D\text{ rel}}$), $\phi_{A\text{ color}}$ ($\phi_{B\text{ color}}$, $\phi_{C\text{ color}}$, $\phi_{D\text{ color}}$), $\phi_{A\text{ flavor}}$ ($\phi_{B\text{ flavor}}$, $\phi_{C\text{ flavor}}$, $\phi_{D\text{ flavor}}$), and $\chi_{S_A S_{A_z}}$ ($\chi_{S_B S_{B_z}}$, $\chi_{S_C S_{C_z}}$, $\chi_{S_D S_{D_z}}$) are the quark-antiquark relative-motion wave function, the color wave function, the flavor wave function, and the spin wave function of meson A (B , C , D), respectively. The spin of meson A (B , C , D) is S_A (S_B , S_C , S_D) with its magnetic projection quantum number S_{A_z} (S_{B_z} , S_{C_z} , S_{D_z}). The transition amplitudes contain color, spin, and flavor matrix elements. The color matrix element is

$$\mathcal{M}_{a\bar{q}_1\bar{q}_2c} = \phi_{C\text{ color}}^+ \phi_{D\text{ color}}^+ \frac{\vec{\lambda}(34)}{2} \cdot \frac{\vec{\lambda}(21)}{2} \phi_{A\text{ color}} \phi_{B\text{ color}} = \frac{4}{9}, \quad (56)$$

for the left diagram of Fig. 1, and

$$\mathcal{M}_{a\bar{q}_1\bar{q}_2c} = \phi_{C\text{ color}}^+ \phi_{D\text{ color}}^+ \frac{\vec{\lambda}(34)}{2} \cdot \frac{\vec{\lambda}(12)}{2} \phi_{A\text{ color}} \phi_{B\text{ color}} = \frac{4}{9}, \quad (57)$$

for the right diagram of Fig. 1. The transition potential in Eq. (41) includes the Pauli matrices $\vec{\sigma}(21)$ and $\vec{\sigma}(34)$. The transition amplitudes contain the spin matrix elements $\chi_{S_C S_{C_z}}^+ \chi_{S_D S_{D_z}}^+ P_\sigma \chi_{S_A S_{A_z}} \chi_{S_B S_{B_z}}$. As to the left diagram P_σ is a 2×2 unit matrix, $\sigma_1(21)$, $\sigma_2(21)$, $\sigma_3(21)$, $\sigma_1(34)$, $\sigma_2(34)$, $\sigma_3(34)$, $\sigma_1(21)\sigma_1(34)$, $\sigma_1(21)\sigma_2(34)$, $\sigma_1(21)\sigma_3(34)$, $\sigma_2(21)\sigma_1(34)$, $\sigma_2(21)\sigma_2(34)$, $\sigma_2(21)\sigma_3(34)$, $\sigma_3(21)\sigma_1(34)$, $\sigma_3(21)\sigma_2(34)$, or $\sigma_3(21)\sigma_3(34)$. The spin matrix elements corresponding to the left diagram are listed in Tables 1–14 in Ref. [14]. The matrix elements of $\sigma_1(21)$, $\sigma_3(21)$, $\sigma_1(34)$, $\sigma_3(34)$, $\sigma_1(21)\sigma_1(34)$, $\sigma_1(21)\sigma_3(34)$, $\sigma_2(21)\sigma_2(34)$, $\sigma_3(21)\sigma_1(34)$, and $\sigma_3(21)\sigma_3(34)$ are real, and the matrix elements of $\sigma_2(21)$, $\sigma_2(34)$, $\sigma_1(21)\sigma_2(34)$, $\sigma_2(21)\sigma_1(34)$, $\sigma_2(21)\sigma_3(34)$, and $\sigma_3(21)\sigma_2(34)$ are pure imaginary or zero. The spin matrix elements for the right diagram in Fig. 1 can be obtained from the ones for the left diagram. The real (imaginary) spin matrix elements of $\mathcal{M}_{a\bar{q}_1\bar{q}_2}$ equal the real spin matrix elements (equal the negative of the imaginary spin matrix elements) of $\mathcal{M}_{a\bar{q}_1\bar{q}_2}$, while none, two, or four of the initial and final mesons have zero spins. The real (imaginary) spin matrix elements of $\mathcal{M}_{a\bar{q}_1\bar{q}_2}$ equal the negative of the real spin matrix elements (equal the imaginary spin matrix elements) of $\mathcal{M}_{a\bar{q}_1\bar{q}_2}$, when one or three of the initial and final mesons have zero spins.

The flavor states, $\phi_{A\text{ flavor}}$ and $\phi_{B\text{ flavor}}$, are coupled to the flavor state $|AB, I, I_z\rangle$ with the total isospin I and its magnetic projection quantum number I_z . $\phi_{C\text{ flavor}}$ and $\phi_{D\text{ flavor}}$ are coupled to $|CD, I, I_z\rangle$. The flavor matrix element is

TABLE I. Flavor matrix elements.

Channel	$\mathcal{M}_{aq_1\bar{q}_2f}$	$\mathcal{M}_{a\bar{q}_1q_2f}$
$I = 1 \pi\pi \rightarrow \rho\rho$	1	1
$I = 0 \pi\pi \rightarrow \rho\rho$	$\frac{3}{2}$	$\frac{3}{2}$
$I = 1 K\bar{K} \rightarrow K^*\bar{K}^*$	0	1
$I = 0 K\bar{K} \rightarrow K^*\bar{K}^*$	2	1
$I = 1 K\bar{K}^* \rightarrow K^*\bar{K}^*$	0	1
$I = 0 K\bar{K}^* \rightarrow K^*\bar{K}^*$	2	1
$I = 1 K^*\bar{K} \rightarrow K^*\bar{K}^*$	0	1
$I = 0 K^*\bar{K} \rightarrow K^*\bar{K}^*$	2	1
$I = 1 \pi\pi \rightarrow K\bar{K}$	0	-1
$I = 0 \pi\pi \rightarrow K\bar{K}$	0	$-\frac{\sqrt{6}}{2}$
$I = 1 \pi\rho \rightarrow K\bar{K}^*$	0	-1
$I = 0 \pi\rho \rightarrow K\bar{K}^*$	0	$-\frac{\sqrt{6}}{2}$
$I = 1 \pi\rho \rightarrow K^*\bar{K}$	0	-1
$I = 0 \pi\rho \rightarrow K^*\bar{K}$	0	$-\frac{\sqrt{6}}{2}$
$I = 1 K\bar{K} \rightarrow \rho\rho$	0	-1
$I = 0 K\bar{K} \rightarrow \rho\rho$	0	$-\frac{\sqrt{6}}{2}$

$$\mathcal{M}_{aq_1\bar{q}_2f} = \langle CD, I, I_z | P_{q_1+\bar{q}_2 \rightarrow q_3+\bar{q}_4} | AB, I, I_z \rangle, \quad (58)$$

for the left diagram of Fig. 1, and

$$\mathcal{M}_{a\bar{q}_1q_2f} = \langle CD, I, I_z | P_{\bar{q}_1+q_2 \rightarrow q_3+\bar{q}_4} | AB, I, I_z \rangle, \quad (59)$$

for the right diagram of Fig. 1. The symbol $P_{q_1+\bar{q}_2 \rightarrow q_3+\bar{q}_4}$ ($P_{\bar{q}_1+q_2 \rightarrow q_3+\bar{q}_4}$) is the operator that implements $q_1 + \bar{q}_2 \rightarrow q_3 + \bar{q}_4$ ($\bar{q}_1 + q_2 \rightarrow q_3 + \bar{q}_4$) in flavor space. $\mathcal{M}_{a\bar{q}_1q_2f}$ may differ from $\mathcal{M}_{aq_1\bar{q}_2f}$. In Table I the flavor matrix elements for the reactions are listed:

$$\begin{aligned} \pi\pi &\rightarrow \rho\rho, \quad K\bar{K} \rightarrow K^*\bar{K}^*, \quad K\bar{K}^* \rightarrow K^*\bar{K}^*, \\ K^*\bar{K} &\rightarrow K^*\bar{K}^*, \quad \pi\pi \rightarrow K\bar{K}, \quad \pi\rho \rightarrow K\bar{K}^*, \\ \pi\rho &\rightarrow K^*\bar{K}, \quad K\bar{K} \rightarrow \rho\rho. \end{aligned}$$

We use the following notation, $K = \binom{K^+}{K^0}$, $\bar{K} = \binom{\bar{K}^0}{K^-}$, $K^* = \binom{K^{*+}}{K^{*0}}$, and $\bar{K}^* = \binom{\bar{K}^{*0}}{K^{*-}}$. Let us give an example that shows how to obtain the flavor matrix elements listed in Table I. The example is $\pi\pi \rightarrow K\bar{K}$ for $I = 1$. The initial and final flavor states are given by

$$|\pi\pi, I = 1, I_z = -1\rangle = \frac{1}{\sqrt{2}}(|\pi^0\rangle|\pi^-\rangle - |\pi^-\rangle|\pi^0\rangle), \quad (60)$$

$$|\pi\pi, I = 1, I_z = 0\rangle = \frac{1}{\sqrt{2}}(|\pi^+\rangle|\pi^-\rangle - |\pi^-\rangle|\pi^+\rangle), \quad (61)$$

$$|\pi\pi, I = 1, I_z = 1\rangle = \frac{1}{\sqrt{2}}(|\pi^+\rangle|\pi^0\rangle - |\pi^0\rangle|\pi^+\rangle), \quad (62)$$

$$|K\bar{K}, I = 1, I_z = -1\rangle = |K^0\rangle|K^-\rangle, \quad (63)$$

$$|K\bar{K}, I = 1, I_z = 0\rangle = \frac{1}{\sqrt{2}}(|K^+\rangle|K^-\rangle + |K^0\rangle|\bar{K}^0\rangle), \quad (64)$$

$$|K\bar{K}, I = 1, I_z = 1\rangle = |K^+\rangle|\bar{K}^0\rangle. \quad (65)$$

The flavor wave functions of the pion and kaon are $|\pi^+\rangle = -|u\bar{d}\rangle$, $|\pi^0\rangle = \frac{1}{\sqrt{2}}(|u\bar{u}\rangle - |d\bar{d}\rangle)$, $|\pi^-\rangle = |d\bar{u}\rangle$, $|K^+\rangle = |u\bar{s}\rangle$, $|K^0\rangle = |d\bar{s}\rangle$, $|\bar{K}^0\rangle = -|s\bar{d}\rangle$, $|K^-\rangle = |s\bar{u}\rangle$. The flavor matrix elements for $\pi\pi \rightarrow K\bar{K}$ for $I = 1$ are $\mathcal{M}_{aq_1\bar{q}_2f} = 0$ and $\mathcal{M}_{a\bar{q}_1q_2f} = -1$, which are independent of I_z . This indicates that only the right diagram in Fig. 1 contributes to $\pi\pi \rightarrow K\bar{K}$ for $I = 1$.

V. QUARK-ANTIQUARK RELATIVE-MOTION WAVE FUNCTIONS

The mesonic quark-antiquark relative-motion wave functions in coordinate space are solutions of the Schrödinger equation with the potential between constituents a and b in the medium [15]:

$$V_{ab}(\vec{r}) = V_{si}(\vec{r}) + V_{ss}(\vec{r}), \quad (66)$$

where \vec{r} is the relative coordinate of a and b . V_{si} is the central spin-independent potential,

$$\begin{aligned} V_{si}(\vec{r}) = & -\frac{\vec{\lambda}_a}{2} \cdot \frac{\vec{\lambda}_b}{2} \frac{3}{4} D \left[1.3 - \left(\frac{T}{T_c} \right)^4 \right] \tanh(Ar) \\ & + \frac{\vec{\lambda}_a}{2} \cdot \frac{\vec{\lambda}_b}{2} \frac{6\pi v(\lambda r)}{25} \frac{v(\lambda r)}{r} \exp(-Er), \end{aligned} \quad (67)$$

where $D = 0.7$ GeV, $T_c = 0.175$ GeV, $A = 1.5[0.75 + 0.25(T/T_c)^{10}]^6$ GeV, $E = 0.6$ GeV, $\lambda = \sqrt{25/16\pi^2\alpha'}$ with $\alpha' = 1.04$ GeV $^{-2}$, $\vec{\lambda}_a$ are the Gell-Mann matrices for the color generators of constituent a , and $v(x)$ is

$$v(x) = \frac{100}{3\pi} \int_0^\infty \frac{dQ}{Q} \left[\rho(\vec{Q}^2) - \frac{K}{\vec{Q}^2} \right] \sin\left(\frac{Q}{\lambda}x\right), \quad (68)$$

where $K = 3/16\pi^2\alpha'$ and $\rho(\vec{Q}^2)$ is given by Buchmüller and Tye [16]. At short distances the quark interaction is described by perturbative QCD in vacuum, and one-gluon exchange plus perturbative one- and two-loop corrections gives the quark-antiquark potential $-\frac{8\pi}{25} \frac{v(\lambda r)}{r}$ [16]. Medium screening sets in at distances $r \geq 0.3$ fm. Including medium effects lattice QCD calculations have provided the numerical quark-antiquark potential at intermediate and long distances [17], which depends on the temperature of the medium. The potential $V_{si}(\vec{r})$ fits rather well $-\frac{8\pi}{25} \frac{v(\lambda r)}{r}$ at short distances and the numerical potential at intermediate and long distances.

Starting with Feynman diagrams for elastic particle-particle scattering, one gets a relativistic particle-particle potential. Application of the Foldy-Wouthuysen canonical transformation to the two-particle relativistic Hamiltonian with the relativistic potential leads to a nonrelativistic particle-particle potential that includes a central spin-independent potential, a spin-spin interaction, and other terms [18]. This standard procedure for obtaining the nonrelativistic particle-particle potential is the same for heavy or light particles. In other words, the particle-particle potential is valid no matter how light the particles are. This procedure has been successfully applied and tested to get the electron-electron potential arising from propagation of a spacelike photon [19], the short-distance quark-quark potential arising from propagation of a spacelike gluon [20], and so on. Thus, the first term in Eq. (67), obtained in lattice calculations involving a heavy quark and a heavy antiquark, is reasonably applied to a light constituent quark and a light constituent antiquark as well.

The second term in Eq. (66) is the spin-spin interaction that arises from perturbative one-gluon exchange plus one- and two-loop corrections [21] and includes relativistic effects [3,22]:

$$V_{ss}(\vec{r}) = -\frac{\vec{\lambda}_a}{2} \cdot \frac{\vec{\lambda}_b}{2} \frac{16\pi^2}{25} \frac{d^3}{\pi^{3/2}} \exp(-d^2 r^2) \frac{\vec{s}_a \cdot \vec{s}_b}{m_a m_b} + \frac{\vec{\lambda}_a}{2} \cdot \frac{\vec{\lambda}_b}{2} \frac{4\pi}{25} \frac{1}{r} \frac{d^2 v(\lambda r)}{dr^2} \frac{\vec{s}_a \cdot \vec{s}_b}{m_a m_b}, \quad (69)$$

where \vec{s}_a is the spin of constituent a , and the quantity d is given by

$$d^2 = d_1^2 \left[\frac{1}{2} + \frac{1}{2} \left(\frac{4m_a m_b}{(m_a + m_b)^2} \right)^4 \right] + d_2^2 \left(\frac{2m_a m_b}{m_a + m_b} \right)^2, \quad (70)$$

where $d_1 = 0.15$ GeV and $d_2 = 0.705$.

With up quark mass 0.32 GeV, down quark mass 0.32 GeV, strange quark mass 0.5 GeV, and charm quark mass 1.51 GeV, the Schrödinger equation with the potential given in Eq. (66) at $T = 0$ is solved to reproduce the experimental masses of π , ρ , K , K^* , J/ψ , ψ' , χ_c , D , D^* , D_s , and D_s^* mesons [23]. The elastic $\pi\pi$ scattering for $I = 2$ is governed by the quark-interchange process. The experimental data of S-wave phase shifts for the scattering in vacuum [24–27] are reproduced in the Born approximation together with the pionic quark-antiquark relative-motion wave functions obtained from the Schrödinger equation [15].

VI. NUMERICAL CROSS SECTIONS AND DISCUSSIONS

We are now ready to calculate elastic phase shifts for $\pi\pi$ scattering in vacuum. From the transition amplitudes we get the reduced T -matrix element,

$$T_{fi} = \frac{\mathcal{M}_{aq_1\bar{q}_2} + \mathcal{M}_{a\bar{q}_1q_2}}{(2\pi)^3 \sqrt{2E_A 2E_B 2E_C 2E_D}}. \quad (71)$$

The phase shift for $A + B \rightarrow A + B$ is

$$\exp(i\delta_l) \sin \delta_l = -\frac{2\pi^2 |\vec{P}| E_A E_B}{E_A + E_B} \int_{-1}^1 dx T_{fi} P_l(x), \quad (72)$$

where $x = \cos \theta$, and P_l are the Legendre polynomials. The elastic phase shift is calculated by the expression

$$\delta_l = -\frac{1}{2} \arcsin \text{Re} \left[\frac{4\pi^2 |\vec{P}| E_A E_B}{E_A + E_B} \int_{-1}^1 dx T_{fi} P_l(x) \right]. \quad (73)$$

The P -wave $I = 1$ elastic phase shifts for $\pi\pi$ scattering in vacuum are shown in Fig. 3 and compared with the experimental data [28–36].

The S -wave elastic $\pi\pi$ scattering for $I = 0$ is governed by not only the quark-antiquark annihilation but also antiquark interchange (or quark interchange) shown in Figs. 4 and 5. The four diagrams in Fig. 4 show meson-meson scattering in the prior form which means that gluon exchange occurs before antiquark interchange. The corresponding transition amplitude is denoted by $\mathcal{M}_{fi}^{\text{prior}}$. The four diagrams in Fig. 5 show meson-meson scattering in the post form which contains gluon exchange after antiquark interchange. The corresponding transition amplitude is denoted by $\mathcal{M}_{fi}^{\text{post}}$. $\mathcal{M}_{fi}^{\text{post}}$ may differ from $\mathcal{M}_{fi}^{\text{prior}}$ [37–39], but the difference disappears since the potential in Eq. (66) and the mesonic quark-antiquark relative-motion wave functions obtained in Sec. V are used to get $\mathcal{M}_{fi}^{\text{prior}}$ and $\mathcal{M}_{fi}^{\text{post}}$ according to Eqs. (2) and (3) in Ref. [15]. Finally, $(\mathcal{M}_{fi}^{\text{prior}} + \mathcal{M}_{fi}^{\text{post}})/2$ is added to $\mathcal{M}_{aq_1\bar{q}_2} + \mathcal{M}_{a\bar{q}_1q_2}$

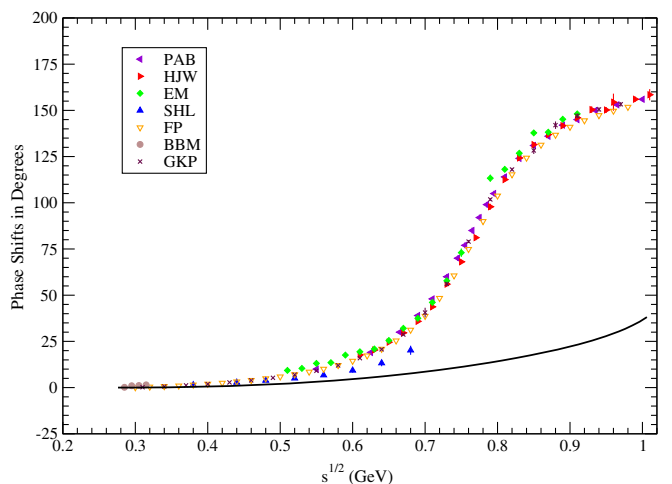


FIG. 3. P -wave $I = 1$ elastic phase shifts for $\pi\pi$ scattering. The solid curve is the present theoretical result. Experimental data: \triangleleft , Ref. [28]; \triangleright , Ref. [29]; \diamond , Ref. [30]; \triangle , Ref. [31]; ∇ , Ref. [33]; \circ , Ref. [34]; \times , Ref. [36].

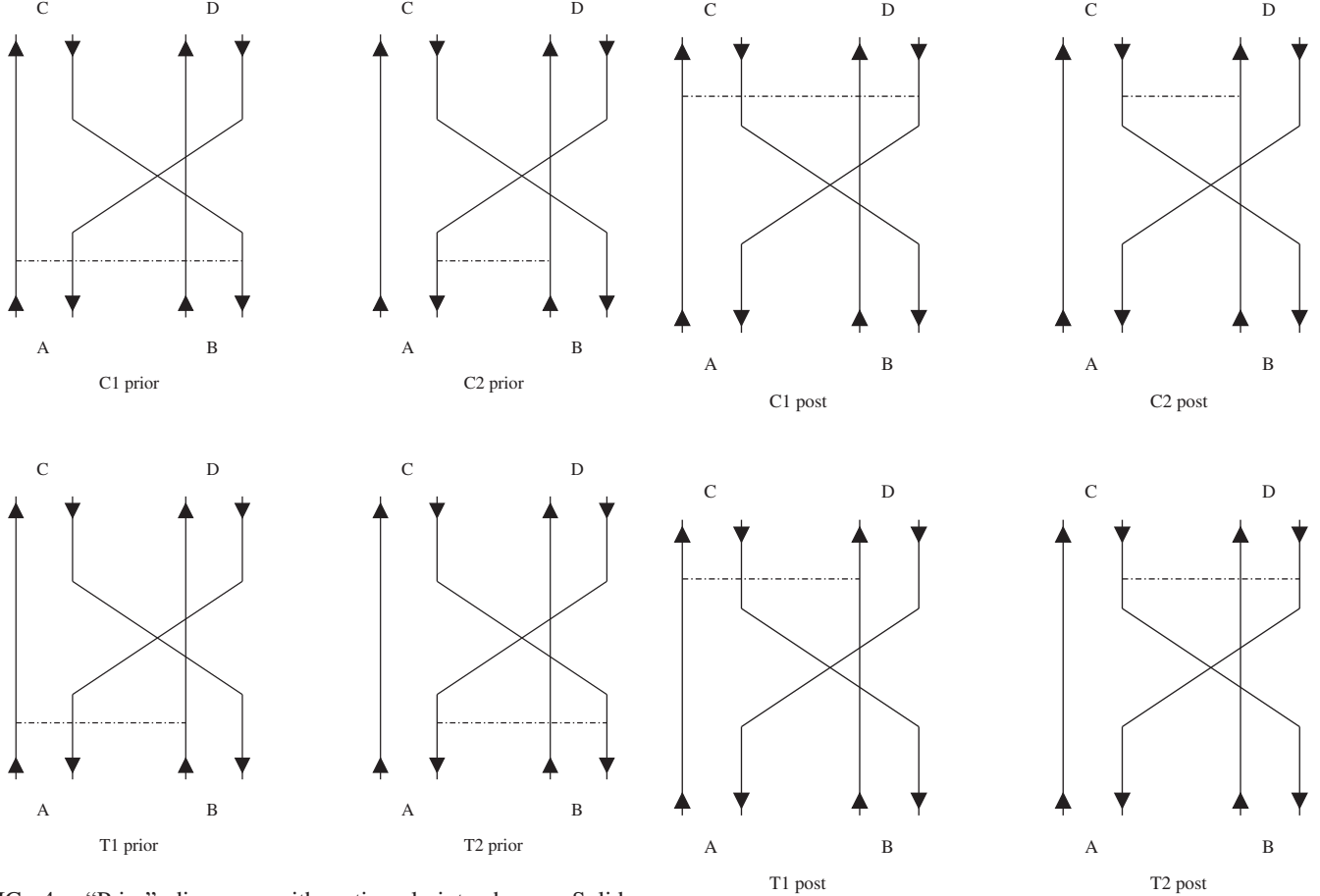


FIG. 4. “Prior” diagrams with antiquark interchange. Solid (dot-dashed) lines represent quarks or antiquarks (interaction).

in Eq. (71) to calculate S -wave $I = 0$ elastic phase shifts for $\pi\pi$ scattering in vacuum by Eq. (73). Numerical phase shifts are shown in Fig. 6.

When the S -wave $I = 0$ elastic phase shift is larger than 30 degrees, it increases rapidly with increasing \sqrt{s} . This behavior is already known from results of chiral perturbation theory [40,41] and the result of the master formula approach [42]. The experimental data of P -wave $I = 1$ elastic phase shifts for $\pi\pi$ scattering in vacuum cannot be reproduced. This is because resonances are not included in the present approach. This is similar to the tree calculation in chiral perturbation theory [40]. Including one- and two-loop corrections in chiral perturbation theory and imposing unitarity, the resonances appear and the experimental data are reproduced. This has been shown in approaches based on the results of chiral perturbation theory, for example, the master formula approach [42], the Padé method [43], the large- N_f expansion [44], the N/D method [45], the inverse amplitude method [46], the K -matrix method [47], the current algebra unitarization [48], the Roy equations [49], the coupled-channel Lippmann-Schwinger equations [50], the Bethe-Salpeter approach [51], and the approaches based on effective meson Lagrangians [52–59].

FIG. 5. “Post” diagrams with antiquark interchange. Solid (dot-dashed) lines represent quarks or antiquarks (interaction).

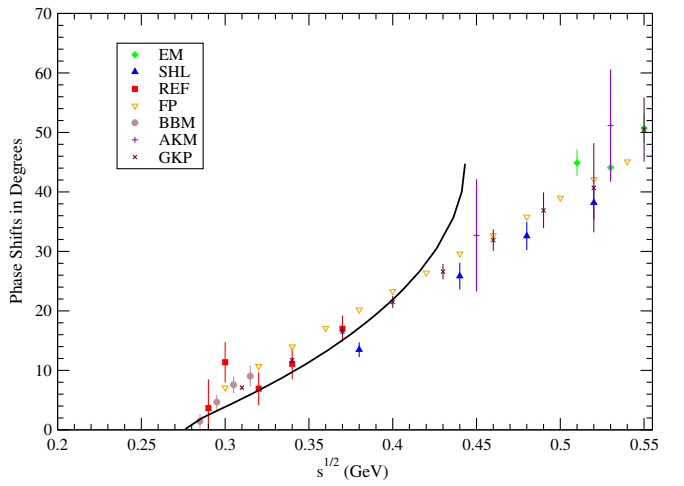


FIG. 6. S -wave $I = 0$ elastic phase shifts for $\pi\pi$ scattering. The solid curve is the present theoretical result. Experimental data: \diamond , Ref. [30]; \triangle , Ref. [31]; \square , Ref. [32]; ∇ , Ref. [33]; \circ , Ref. [34]; $+$, Ref. [35]; \times , Ref. [36].

We consider the following inelastic meson-meson scattering processes that are governed by quark-antiquark annihilation and creation:

$$\begin{aligned} I = 1 \pi\pi &\rightarrow \rho\rho, & K\bar{K} &\rightarrow K^*\bar{K}^*, & K\bar{K}^* &\rightarrow K^*\bar{K}^*, \\ K^*\bar{K} &\rightarrow K^*\bar{K}^*, \\ I = 1 \pi\pi &\rightarrow K\bar{K}, & \pi\rho &\rightarrow K\bar{K}^*, & \pi\rho &\rightarrow K^*\bar{K}, \\ K\bar{K} &\rightarrow \rho\rho. \end{aligned}$$

The quark-antiquark relative-motion wave functions, $\phi_{A\text{rel}}$, $\phi_{B\text{rel}}$, $\phi_{C\text{rel}}$, and $\phi_{D\text{rel}}$, are obtained from the Schrödinger equation with the potential given in Eq. (66). With the transition potential and the wave functions in Eqs. (52)–(55), we calculate the transition amplitudes, $\mathcal{M}_{a\bar{q}_1\bar{q}_2}$ and $\mathcal{M}_{a\bar{q}_1q_2}$. According to Eq. (34) we calculate unpolarized cross sections at the six temperatures $T/T_c = 0$, 0.65, 0.75, 0.85, 0.9, and 0.95. In Figs. 7–15 we plot the unpolarized cross sections for the nine channels:

$$\begin{aligned} I = 1 \pi\pi &\rightarrow \rho\rho, & I = 1 K\bar{K} &\rightarrow K^*\bar{K}^*, \\ I = 0 K\bar{K} &\rightarrow K^*\bar{K}^*, & I = 1 K\bar{K}^* &\rightarrow K^*\bar{K}^*, \\ I = 0 K\bar{K}^* &\rightarrow K^*\bar{K}^*, & I = 1 \pi\pi &\rightarrow K\bar{K}, \\ I = 1 \pi\rho &\rightarrow K\bar{K}^*, & I = 1 \pi\rho &\rightarrow K^*\bar{K}, \\ I = 1 K\bar{K} &\rightarrow \rho\rho. \end{aligned}$$

Depending on temperature, a reaction is either endothermic or exothermic. The numerical cross sections for endothermic reactions are parametrized as

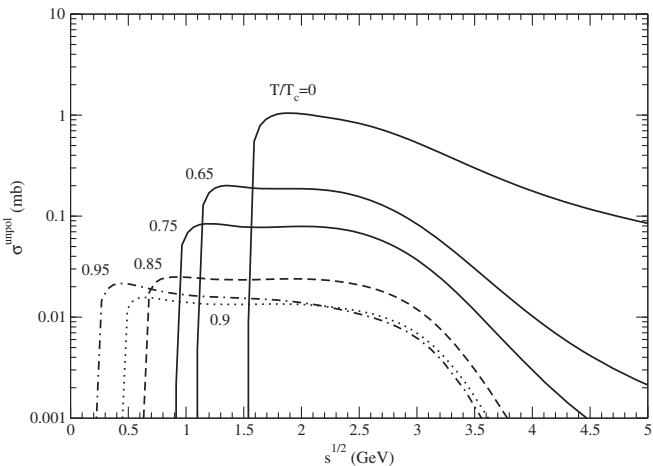


FIG. 7. Cross sections for $\pi\pi \rightarrow \rho\rho$ for $I = 1$ at various temperatures.

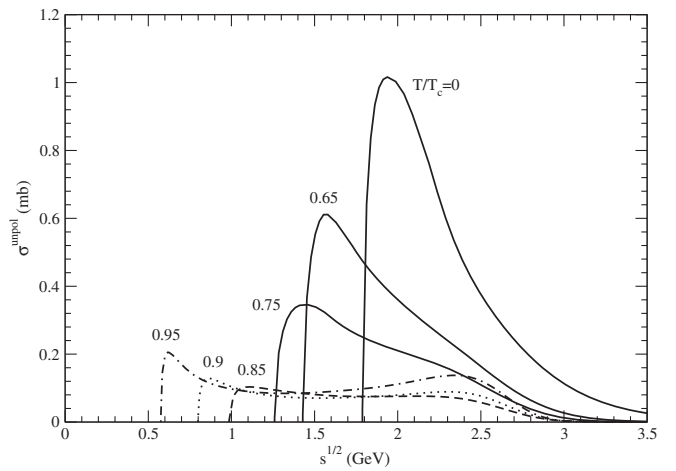


FIG. 8. Cross sections for $K\bar{K} \rightarrow K^*\bar{K}^*$ for $I = 1$ at various temperatures.

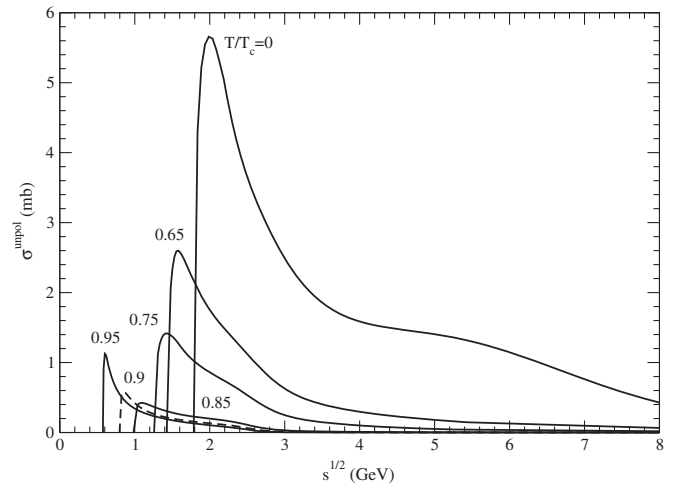


FIG. 9. Cross sections for $K\bar{K} \rightarrow K^*\bar{K}^*$ for $I = 0$ at various temperatures.

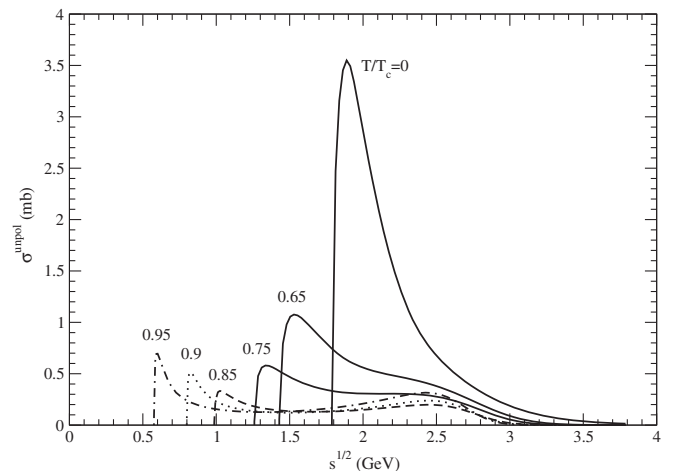


FIG. 10. Cross sections for $K\bar{K}^* \rightarrow K^*\bar{K}^*$ for $I = 1$ at various temperatures.

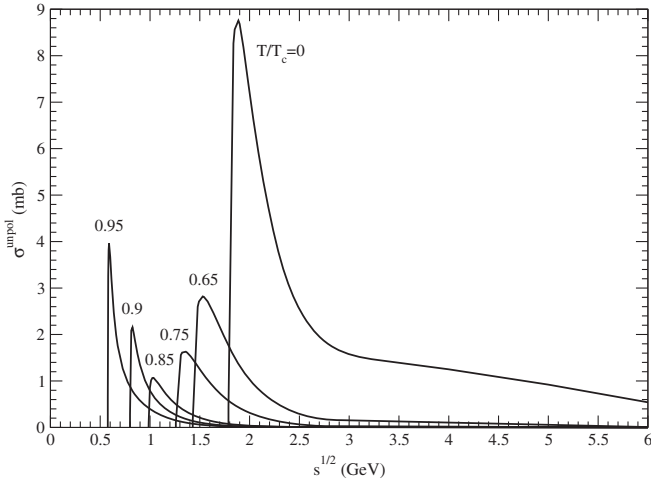


FIG. 11. Cross sections for $K\bar{K}^* \rightarrow K^*\bar{K}^*$ for $I = 0$ at various temperatures.

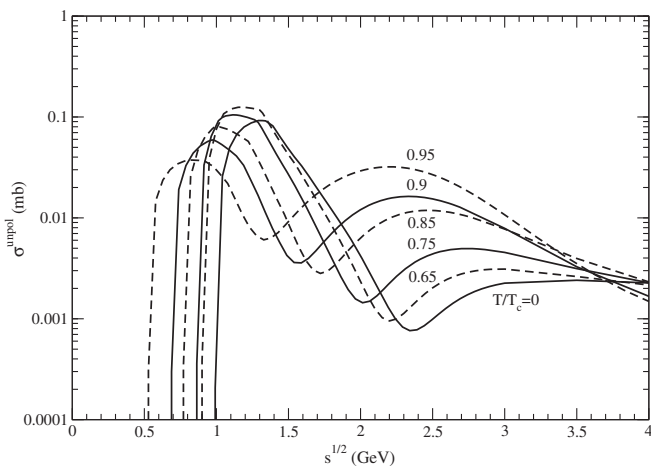


FIG. 12. Cross sections for $\pi\pi \rightarrow K\bar{K}$ for $I = 1$ at various temperatures.

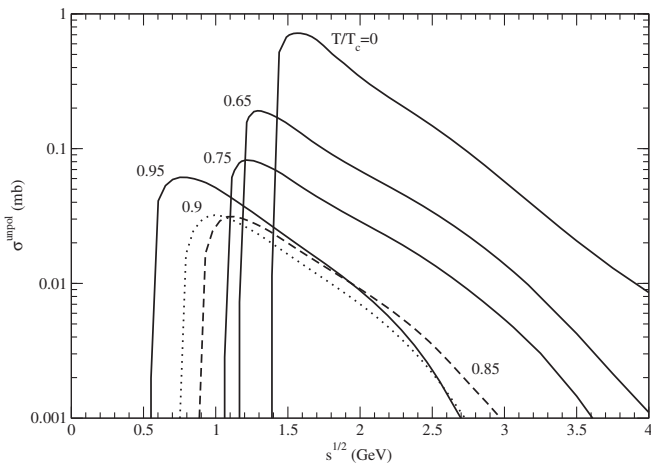


FIG. 13. Cross sections for $\pi\rho \rightarrow K\bar{K}^*$ for $I = 1$ at various temperatures.

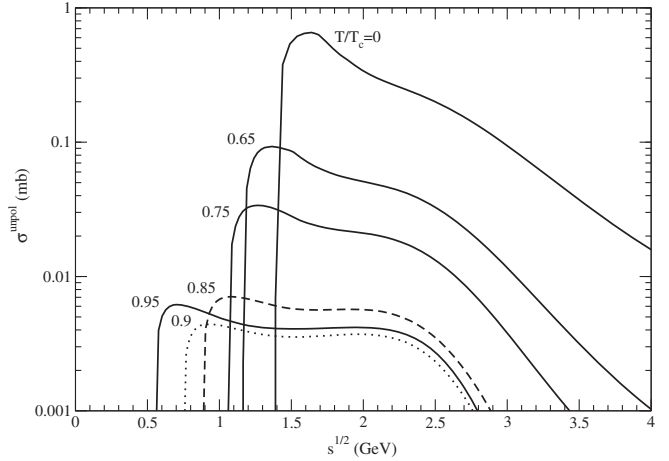


FIG. 14. Cross sections for $\pi\rho \rightarrow K^*\bar{K}$ for $I = 1$ at various temperatures.

$$\begin{aligned} \sigma^{\text{unpol}}(\sqrt{s}, T) = & a_1 \left(\frac{\sqrt{s} - \sqrt{s_0}}{b_1} \right)^{e_1} \\ & \times \exp \left[e_1 \left(1 - \frac{\sqrt{s} - \sqrt{s_0}}{b_1} \right) \right] \\ & + a_2 \left(\frac{\sqrt{s} - \sqrt{s_0}}{b_2} \right)^{e_2} \\ & \times \exp \left[e_2 \left(1 - \frac{\sqrt{s} - \sqrt{s_0}}{b_2} \right) \right], \end{aligned} \quad (74)$$

where $\sqrt{s_0}$ is the threshold energy, and a_1, b_1, e_1, a_2, b_2 , and e_2 are parameters. The numerical cross sections for exothermic reactions are parametrized as

$$\begin{aligned} \sigma^{\text{unpol}}(\sqrt{s}, T) = & \frac{\vec{P}'^2}{\vec{P}^2} \left\{ a_1 \left(\frac{\sqrt{s} - \sqrt{s_0}}{b_1} \right)^{e_1} \right. \\ & \times \exp \left[e_1 \left(1 - \frac{\sqrt{s} - \sqrt{s_0}}{b_1} \right) \right] \\ & + a_2 \left(\frac{\sqrt{s} - \sqrt{s_0}}{b_2} \right)^{e_2} \\ & \left. \times \exp \left[e_2 \left(1 - \frac{\sqrt{s} - \sqrt{s_0}}{b_2} \right) \right] \right\}. \end{aligned} \quad (75)$$

The parameter values are listed in Tables II–IV. As in Ref. [2], we also list the quantities d_0 and $\sqrt{s_z}$; d_0 is the separation between the peak's location on the \sqrt{s} -axis and the threshold energy, and $\sqrt{s_z}$ is the square root of the Mandelstam variable at which the cross section is 1/100 of the peak cross section.

In the temperature region that is covered by hadronic matter produced in ultrarelativistic heavy-ion collisions, the central spin-independent potential given in Eq. (67) at long distances becomes independent of distance and exhibits a plateau. Confinement is marked by the plateau. With

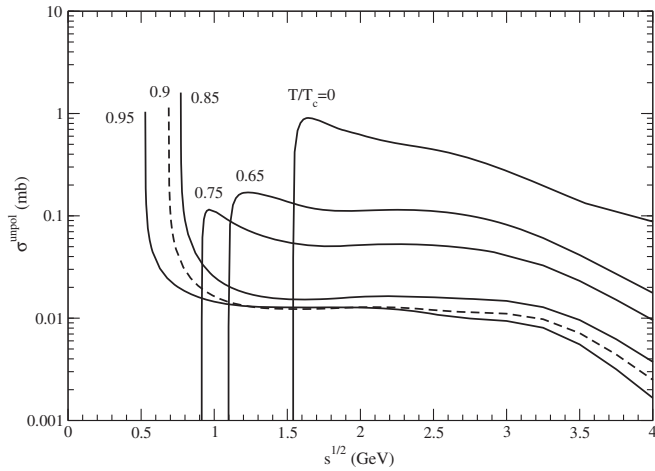


FIG. 15. Cross sections for $K\bar{K} \rightarrow \rho\rho$ for $I = 1$ at various temperatures.

increasing temperature the height of the plateau decreases, confinement becomes weaker and weaker, and quark-antiquark bound states become looser and looser. Increasing radii of mesons A and B cause increasing cross sections for meson-meson reactions. Weakening confinement causes the combination of final quarks and antiquarks in forming mesons C and D to be more difficult, thus decreasing cross sections for meson-meson reactions.

The two factors determine the decrease or the increase of peak cross sections of endothermic reactions shown in Figs. 7–15. For example, from $T/T_c = 0$ to 0.85 and near the threshold energy the increase of the cross section due to increasing radii of initial mesons cannot overcome the decrease of the cross section due to weakening confinement. Thus, the peak cross section of $K\bar{K} \rightarrow K^*\bar{K}^*$ decreases. In contrast, the peak cross section of $K\bar{K} \rightarrow K^*\bar{K}^*$ increases as temperature goes from $T/T_c = 0.85$ to 0.95. In vacuum the ρ mass is larger than the kaon mass. When the temperature increases, the ρ mass decreases faster than the kaon mass. At $T \approx 0.785T_c$ the ρ mass equals the kaon mass. Below this temperature the reaction $K\bar{K} \rightarrow \rho\rho$ for $I = 1$ in Fig. 15 is endothermic; otherwise, it is exothermic. When temperature increases from $T/T_c = 0.6$ to 1, the π , ρ , K , and K^* masses decrease. The threshold energies shown in Figs. 7–15 thus decrease. The ratio of the peak cross section at $T/T_c = 0.75$ to the peak cross section at $T/T_c = 0$ is 0.08, 0.34, 0.25, 0.16, 0.19, 0.11, 0.05, and 0.13 for $\pi\pi \rightarrow \rho\rho$ for $I = 1$, $K\bar{K} \rightarrow K^*\bar{K}^*$ for $I = 1$, $K\bar{K} \rightarrow K^*\bar{K}^*$ for $I = 0$, $K\bar{K}^* \rightarrow K^*\bar{K}^*$ for $I = 1$, $K\bar{K}^* \rightarrow K^*\bar{K}^*$ for $I = 0$, $\pi\rho \rightarrow K\bar{K}^*$ for $I = 1$, $\pi\rho \rightarrow K^*\bar{K}$ for $I = 1$, and $K\bar{K} \rightarrow \rho\rho$ for $I = 1$, respectively. Clearly, the cross sections have remarkable dependence on temperature.

It is shown in Table I that the two diagrams in Fig. 1 contribute to $K\bar{K} \rightarrow K^*\bar{K}^*$ for $I = 0$ and $K\bar{K}^* \rightarrow K^*\bar{K}^*$ for

TABLE II. Values of the parameters. a_1 and a_2 are in units of millibarns; b_1 , b_2 , d_0 , and $\sqrt{s_z}$ are in units of GeV; e_1 and e_2 are dimensionless.

Reactions	T/T_c	a_1	b_1	e_1	a_2	b_2	e_2	d_0	$\sqrt{s_z}$
$I = 1 \pi\pi \rightarrow \rho\rho$	0	0.19	1.4	4.2	1.08	0.35	0.67	0.35	7.76
	0.65	0.11	1.3	6.8	0.2	0.27	0.54	0.25	5.05
	0.75	0.042	1.46	10.55	0.086	0.34	0.51	0.25	4.57
	0.85	0.015	1.69	12.6	0.027	0.35	0.48	0.3	4.13
	0.9	0.0085	1.84	9.13	0.0166	0.3	0.45	0.2	4.01
	0.95	0.0089	1.9	6.9	0.022	0.29	0.48	0.25	3.87
$I = 0 \pi\pi \rightarrow \rho\rho$	0	1.09	0.17	0.65	1.73	0.65	1.04	0.35	7.99
	0.65	0.14	1.36	9.82	0.44	0.34	0.53	0.25	5.1
	0.75	0.125	1.37	6.67	0.172	0.27	0.52	0.3	4.63
	0.85	0.039	1.64	9.76	0.057	0.3	0.47	0.3	4.25
	0.9	0.0334	0.213	0.45	0.024	1.6	3.1	0.2	4.02
	0.95	0.0403	0.54	0.33	0.044	0.038	0.55	0.04	3.79
$I = 1 K\bar{K} \rightarrow K^*\bar{K}^*$	0	0.95	0.13	0.53	0.17	0.48	1.07	0.15	3.81
	0.65	0.6	0.142	0.52	0.133	0.79	4.54	0.15	3.28
	0.75	0.049	1.02	9.24	0.349	0.2	0.49	0.2	3.19
	0.85	0.109	0.145	0.47	0.068	1.12	6.27	0.125	3.19
	0.9	0.121	0.069	0.45	0.082	1.28	1.39	0.071	3.15
	0.95	0.181	0.052	0.43	0.158	5.89	0.5	0.0418	3.03
$I = 0 K\bar{K} \rightarrow K^*\bar{K}^*$	0	1.74	1.3	0.42	4.71	0.186	0.55	0.2	10.36
	0.65	1.45	0.54	0.99	1.87	0.09	0.51	0.15	9.22
	0.75	1.42	0.155	0.51	0.47	0.98	4.04	0.175	8.4
	0.85	0.2	0.83	2.74	0.42	0.1	0.49	0.1126	4.73
	0.9	0.38	0.051	0.61	0.27	0.24	0.31	0.0418	3.3
	0.95	0.75	0.026	0.55	0.51	0.132	0.33	0.025	2.77

TABLE III. The same as Table II, but for three other reactions.

Reactions	T/T_c	a_1	b_1	e_1	a_2	b_2	e_2	d_0	$\sqrt{s_z}$
$I = 1 K\bar{K}^* \rightarrow K^*\bar{K}^*$	0	1.4	0.08	0.8	2.19	0.13	0.45	0.1	3.52
	0.65	0.36	0.87	4.82	1.08	0.11	0.49	0.1	3.33
	0.75	0.6	0.11	0.46	0.29	1.01	6.85	0.075	3.28
	0.85	0.33	0.056	0.43	0.173	1.35	1.56	0.0418	3.18
	0.9	0.48	0.041	0.4	0.22	2.69	0.9	0.025	3.16
	0.95	0.61	0.036	0.36	0.29	3.67	0.92	0.025	3.02
$I = 0 K\bar{K}^* \rightarrow K^*\bar{K}^*$	0	1.4	0.9	2.65	8.9	0.1	0.5	0.1	7.96
	0.65	0.35	0.05	0.72	2.5	0.13	0.45	0.1	5.6
	0.75	0.1	0.61	4.58	1.64	0.1	0.47	0.1	4.15
	0.85	1.08	0.06	0.44	0.09	0.5	2.15	0.05	2.46
	0.9	0.79	0.15	1.49	2.04	0.019	0.47	0.025	1.99
	0.95	0.78	0.18	0.63	3.6	0.017	0.41	0.0126	1.62
$I = 1 \pi\pi \rightarrow K\bar{K}$	0	0.02	0.068	0.82	0.088	0.29	2.83	0.3	2.26
	0.65	0.03	0.06	0.8	0.13	0.28	2.76	0.28	2.1
	0.75	0.04	0.11	0.8	0.09	0.3	3.5	0.25	9.1
	0.85	0.064	0.3	3.89	0.031	0.11	0.76	0.219	7.26
	0.9	0.021	0.092	0.74	0.051	0.3	3.72	0.28	6.32
	0.95	0.0136	0.038	0.75	0.0407	0.29	2.83	0.3	6.17

TABLE IV. The same as Table II, but for three other reactions.

Reactions	T/T_c	a_1	b_1	e_1	a_2	b_2	e_2	d_0	$\sqrt{s_z}$
$I = 1 \pi\rho \rightarrow K\bar{K}^*$	0	0.1	0.96	0.71	0.66	0.16	0.64	0.175	4.08
	0.65	0.048	0.62	0.98	0.17	0.12	0.52	0.125	3.81
	0.75	0.02	0.43	0.38	0.064	0.16	0.57	0.15	3.69
	0.85	0.004	0.54	0.27	0.027	0.25	0.84	0.25	3.36
	0.9	0.0076	0.33	0.38	0.024	0.25	0.92	0.25	3.15
	0.95	0.008	0.22	1.21	0.053	0.22	0.49	0.2	3.05
$I = 1 \pi\rho \rightarrow K^*\bar{K}$	0	0.37	0.17	1.34	0.32	0.36	0.54	0.25	4.67
	0.65	0.034	0.12	1.01	0.065	0.35	0.47	0.2	4.05
	0.75	0.015	0.09	0.5	0.024	0.5	0.71	0.2	3.86
	0.85	0.0074	0.21	0.49	0.004	1.21	8.98	0.2	3.41
	0.9	0.0045	0.19	0.48	0.003	1.29	6.6	0.2	3.25
	0.95	0.0062	0.162	0.48	0.0038	1.39	4.95	0.15	3.18
$I = 1 K\bar{K} \rightarrow \rho\rho$	0	0.77	0.08	0.53	0.49	0.64	1.29	0.11	5.99
	0.65	0.175	0.133	0.49	0.108	1.27	3.6	0.13	5.52
	0.75	0.112	0.065	0.44	0.056	1.08	1.5	0.05	5.28
	0.85	0.021	0.116	0.45	0.0173	1.55	3.44	0.1	4.83
	0.9	0.0117	0.15	0.47	0.0122	1.65	2.89	0.15	4.77
	0.95	0.0068	0.08	0.47	0.0118	1.2	0.79	0.3	4.7

$I = 0$, and only the right diagram contributes to $K\bar{K} \rightarrow K^*\bar{K}^*$ for $I = 1$ and $K\bar{K}^* \rightarrow K^*\bar{K}^*$ for $I = 1$. The peak cross section of $K\bar{K} \rightarrow K^*\bar{K}^*$ ($K\bar{K}^* \rightarrow K^*\bar{K}^*$) for $I = 0$ at a given temperature is more than 2 times the one for $I = 1$. In addition, cross sections for $K^*\bar{K} \rightarrow K^*\bar{K}^*$ equal the cross sections for $K\bar{K}^* \rightarrow K^*\bar{K}^*$.

It is shown in Table I that only the right diagram in Fig. 1 contributes to the reactions, $\pi\pi \rightarrow K\bar{K}$, $\pi\rho \rightarrow K\bar{K}^*$, $\pi\rho \rightarrow K^*\bar{K}$, and $K\bar{K} \rightarrow \rho\rho$. Since the flavor matrix element for the channel $I = 0$ is $-\sqrt{6}/2$ times the one for $I = 1$, the cross section for the channel $I = 0$ is 1.5 times the one for

$I = 1$. Therefore, we only plot the unpolarized cross sections for $\pi\pi \rightarrow K\bar{K}$ for $I = 1$ in Fig. 12, for $\pi\rho \rightarrow K\bar{K}^*$ for $I = 1$ in Fig. 13, for $\pi\rho \rightarrow K^*\bar{K}$ for $I = 1$ in Fig. 14, and for $K\bar{K} \rightarrow \rho\rho$ for $I = 1$ in Fig. 15. The cross section for $\pi\rho \rightarrow K\bar{K}^*$ at $T = 0$ leads to the isospin-averaged cross section that has a maximum value of about 0.36 mb which is close to the one obtained from an effective meson Lagrangian in Refs. [4,6]. Nevertheless, the cross section for $K\bar{K} \rightarrow \rho\rho$ at $T = 0$ provides about 1 mb as the maximum value of the isospin-averaged cross section, which is not close to 3.5 mb given in Refs. [4,6].

The unpolarized cross section for $\pi\pi \rightarrow \rho\rho$ for $I = 2$ has been shown in Fig. 2 of Ref. [2]. The channel is governed by the quark-interchange process. The reaction $\pi\pi \rightarrow \rho\rho$ for $I = 1$ studied in the present work is governed by quark-antiquark annihilation and creation. The unpolarized cross sections for both channels increase rapidly when \sqrt{s} increases from the threshold energy. When \sqrt{s} increases from the magnitude that corresponds to the peak cross section, the cross section for the channel $I = 2$ decreases rapidly, but the one for $I = 1$ decreases slowly. The difference is related to the quark-antiquark relative-motion wave functions of final mesons. The wave functions are exponentially decreasing functions of the quark-antiquark relative momentum. When \sqrt{s} is far away from the threshold energy, the relative momentum of an interchanged quark and an antiquark, which form a final meson in the channel $I = 2$, is usually large [1], but the relative momentum of the quark created from the gluon and an antiquark, which form a final meson in the channel $I = 1$, can still be small. The squared transition amplitude for the reaction with the quark-interchange process at such a value of \sqrt{s} is very small in comparison to the one near the threshold energy, and by contrast the squared transition amplitude for the reaction with the quark-antiquark annihilation is comparable to the one near the threshold energy. Therefore, the cross section has the behavior of rapid decrease for $I = 2$ and of slow decrease for $I = 1$, and the difference between the cross sections for the two channels is large.

The reaction $\pi\pi \rightarrow \rho\rho$ for $I = 0$ involves both quark interchange and quark-antiquark annihilation. The cross section for the reaction including the quark-interchange process in the prior form is

$$\begin{aligned} \sigma_{\text{unpol}}^{\text{prior}}(\sqrt{s}, T) &= \frac{1}{(2J_A + 1)(2J_B + 1)} \frac{1}{32\pi s} \frac{|\vec{P}'(\sqrt{s})|}{|\vec{P}(\sqrt{s})|} \\ &\times \int_0^\pi d\theta \sum_{J_{Az}J_{Bz}J_{Cz}J_{Dz}} \\ &\times |\mathcal{M}_{aq_1\bar{q}_2} + \mathcal{M}_{a\bar{q}_1q_2} + \mathcal{M}_{\text{fi}}^{\text{prior}}|^2 \sin \theta, \end{aligned} \quad (76)$$

where the transition amplitude $\mathcal{M}_{\text{fi}}^{\text{prior}}$ for the process in the prior form is given by Eq. (2) in Ref. [15]. The cross section for the reaction including the quark-interchange process in the post form is

$$\begin{aligned} \sigma_{\text{unpol}}^{\text{post}}(\sqrt{s}, T) &= \frac{1}{(2J_A + 1)(2J_B + 1)} \frac{1}{32\pi s} \frac{|\vec{P}'(\sqrt{s})|}{|\vec{P}(\sqrt{s})|} \\ &\times \int_0^\pi d\theta \sum_{J_{Az}J_{Bz}J_{Cz}J_{Dz}} \\ &\times |\mathcal{M}_{aq_1\bar{q}_2} + \mathcal{M}_{a\bar{q}_1q_2} + \mathcal{M}_{\text{fi}}^{\text{post}}|^2 \sin \theta, \end{aligned} \quad (77)$$

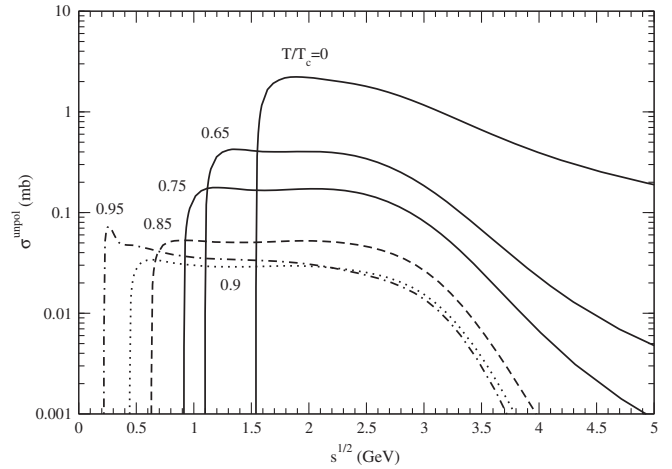


FIG. 16. Cross sections for $\pi\pi \rightarrow \rho\rho$ for $I = 0$ at various temperatures.

where the transition amplitude $\mathcal{M}_{\text{fi}}^{\text{post}}$ for the process in the post form is given by Eq. (3) in Ref. [15]. The unpolarized cross section is given by

$$\sigma_{\text{unpol}}(\sqrt{s}, T) = \frac{1}{2} [\sigma_{\text{unpol}}^{\text{prior}}(\sqrt{s}, T) + \sigma_{\text{unpol}}^{\text{post}}(\sqrt{s}, T)]. \quad (78)$$

Cross sections for the reactions that are governed only by quark interchange have the characteristic that the cross sections rise very rapidly from threshold energies, arrive at maximum values, and decrease rapidly. In other words quark interchange plays a role only near the threshold energy. Therefore, the behavior of the cross section for $\pi\pi \rightarrow \rho\rho$ for $I = 0$ differs from the one for $\pi\pi \rightarrow \rho\rho$ for $I = 1$ near the threshold. This is obvious between the two curves at $T/T_c = 0.95$ in Figs. 7 and 16. It is shown by Table I that the flavor matrix element for $\pi\pi \rightarrow \rho\rho$ for $I = 0$ is 1.5 times the one for $\pi\pi \rightarrow \rho\rho$ for $I = 1$. Therefore, when \sqrt{s} is far away from the threshold, the cross section for $\pi\pi \rightarrow \rho\rho$ for $I = 0$ is nearly 2.25 times the cross section for $\pi\pi \rightarrow \rho\rho$ for $I = 1$.

In order to obtain the cross sections shown in Figs. 7–15, we first calculate the color, spin, and flavor matrix elements of the transition potential given in Eq. (41), next calculate the transition amplitudes according to Eqs. (50) and (51), and finally calculate the unpolarized cross sections by Eq. (34). In the Appendix we provide an alternative way to calculate the transition amplitudes. In this way we apply Fierz transformations to the amplitude in Eq. (39) to get a quark-antiquark potential corresponding to the quark-antiquark annihilation and creation, which is employed to obtain $\mathcal{M}_{aq_1\bar{q}_2}$ and $\mathcal{M}_{a\bar{q}_1q_2}$.

VII. SUMMARY

We have derived the unpolarized cross section for inelastic meson-meson scattering in quark degrees of

freedom. The reactions are governed by quark-antiquark annihilation and creation. The reactions include $\pi\pi \rightarrow \rho\rho$ for $I = 1$, $K\bar{K} \rightarrow K^*\bar{K}^*$, $K\bar{K}^* \rightarrow K^*\bar{K}^*$, $K^*\bar{K} \rightarrow K^*\bar{K}^*$, $\pi\pi \rightarrow K\bar{K}$ for $I = 1$, $\pi\rho \rightarrow K\bar{K}^*$, $\pi\rho \rightarrow K^*\bar{K}$, and $K\bar{K} \rightarrow \rho\rho$. The transition potential corresponding to quark-antiquark annihilation and creation has been derived in perturbative QCD. Some reactions involve only one Feynman diagram at tree level, and the others two. The transition amplitudes including color, spin, and flavor matrix elements are given upon integrating over the relative momenta of the quark and the antiquark of the two initial mesons. The experimental data of S -wave and P -wave elastic phase shifts for $\pi\pi$ scattering near the threshold energy can be accounted for by quark-antiquark annihilation and creation in the Born approximation. Numerical unpolarized cross sections have been obtained at the six temperatures and have shown remarkable temperature dependence. The dependence arises from the quark-antiquark relative-motion wave functions of the initial and final mesons. The numerical cross sections are parametrized for future use in the evolution of hadronic matter.

ACKNOWLEDGMENTS

We thank W. Weise for introducing us to his work and B. S. Zou for helpful discussions on meson-meson reactions. This work was supported by the National Natural Science Foundation of China under Grant No. 11175111.

APPENDIX: TRANSITION AMPLITUDES UNDER THE FIERZ TRANSFORMATIONS

We provide an alternative way to calculate the transition amplitudes $\mathcal{M}_{aq_1\bar{q}_2}$ and $\mathcal{M}_{a\bar{q}_1q_2}$. For this we need the Fierz identity for Dirac matrices and Dirac spinors [60], u_1 , u_2 , u_3 , and u_4 ,

$$\begin{aligned} \bar{u}_1\gamma_\tau u_2\bar{u}_3\gamma^\tau u_4 &= \bar{u}_1u_4\bar{u}_3u_2 - \frac{1}{2}\bar{u}_1\gamma_\tau u_4\bar{u}_3\gamma^\tau u_2 \\ &\quad - \frac{1}{2}\bar{u}_1\gamma_5\gamma_\tau u_4\bar{u}_3\gamma^5\gamma^\tau u_2 - \bar{u}_1\gamma_5u_4\bar{u}_3\gamma^5u_2. \end{aligned} \tag{A1}$$

Let c_1 , c_2 , c_3 , and c_4 (f_1 , f_2 , f_3 , and f_4) be the color (flavor) wave functions of the initial quark, the initial antiquark, the final quark, and the final antiquark in Fig. 2, respectively. We Fierz transform color matrices [61],

$$\begin{aligned} c_3^+\lambda^e c_4 c_2^+ \lambda^e c_1 &= \frac{16}{9} c_3^+ \lambda^0 c_1 c_2^+ \lambda^0 c_4 - \frac{1}{3} c_3^+ \lambda^e c_1 c_2^+ \lambda^e c_4 \\ &= \frac{16}{9} c_3^+ \lambda^0 c_1 c_4^+ \lambda^0 c_2 - \frac{1}{3} c_3^+ \lambda^e c_1 c_4^+ \lambda^{eT} c_2, \end{aligned} \tag{A2}$$

where λ^0 is a 3×3 unit matrix. In terms of the Gell-Mann matrices we Fierz transform flavor matrices in 3-flavor space [61],

$$\begin{aligned} f_3^+\lambda^0 f_4 f_2^+ \lambda^0 f_1 &= \frac{1}{3} f_3^+ \lambda^0 f_1 f_2^+ \lambda^0 f_4 + \frac{1}{2} f_3^+ \lambda^e f_1 f_2^+ \lambda^e f_4 \\ &= \frac{1}{3} f_3^+ \lambda^0 f_1 f_4^+ \lambda^0 f_2 + \frac{1}{2} f_3^+ \lambda^e f_1 f_4^+ \lambda^{eT} f_2. \end{aligned} \tag{A3}$$

This means that the Gell-Mann matrices are also suitable to describe change of light flavors. In Eq. (39) the color and flavor wave functions are suppressed. Explicitly including the wave functions, Eq. (39) is

$$\begin{aligned} \mathcal{M}_a &= f_3^+ \lambda^0 f_4 f_2^+ \lambda^0 f_1 c_3^+ T^e c_4 c_2^+ T^e c_1 \\ &\quad \times \frac{g_s^2}{k^2} \bar{\psi}_{q'}(\vec{p}_3, s_{q'z}) \gamma_\tau \psi_{\bar{q}'}(\vec{p}_4, s_{\bar{q}'z}) \\ &\quad \times \bar{\psi}_{\bar{q}}(\vec{p}_2, s_{\bar{q}z}) \gamma^\tau \psi_q(\vec{p}_1, s_{qz}), \end{aligned} \tag{A4}$$

which is Fierz transformed into

$$\begin{aligned} \mathcal{M}_a &= \left(\frac{1}{3} f_3^+ \lambda^0 f_1 f_2^+ \lambda^0 f_4 + \frac{1}{2} f_3^+ \lambda^e f_1 f_2^+ \lambda^e f_4 \right) \left(\frac{4}{9} c_3^+ \lambda^0 c_1 c_2^+ \lambda^0 c_4 - \frac{1}{12} c_3^+ \lambda^e c_1 c_2^+ \lambda^e c_4 \right) \\ &\quad \times \frac{g_s^2}{k^2} [\bar{\psi}_{q'}(\vec{p}_3, s_{q'z}) \psi_q(\vec{p}_1, s_{qz}) \bar{\psi}_{\bar{q}}(\vec{p}_2, s_{\bar{q}z}) \psi_{\bar{q}'}(\vec{p}_4, s_{\bar{q}'z}) - \frac{1}{2} \bar{\psi}_{q'}(\vec{p}_3, s_{q'z}) \gamma_\tau \psi_q(\vec{p}_1, s_{qz}) \bar{\psi}_{\bar{q}}(\vec{p}_2, s_{\bar{q}z}) \gamma^\tau \psi_{\bar{q}'}(\vec{p}_4, s_{\bar{q}'z}) \\ &\quad - \frac{1}{2} \bar{\psi}_{q'}(\vec{p}_3, s_{q'z}) \gamma_5 \gamma_\tau \psi_q(\vec{p}_1, s_{qz}) \bar{\psi}_{\bar{q}}(\vec{p}_2, s_{\bar{q}z}) \gamma^5 \gamma^\tau \psi_{\bar{q}'}(\vec{p}_4, s_{\bar{q}'z}) - \bar{\psi}_{q'}(\vec{p}_3, s_{q'z}) \gamma_5 \psi_q(\vec{p}_1, s_{qz}) \bar{\psi}_{\bar{q}}(\vec{p}_2, s_{\bar{q}z}) \gamma^5 \psi_{\bar{q}'}(\vec{p}_4, s_{\bar{q}'z})]. \end{aligned} \tag{A5}$$

The amplitude to order of the inverse of the quark mass squared is

$$\begin{aligned}
\mathcal{M}_a = & \frac{g_s^2}{k^2} f_3^+ f_4^+ \left(\frac{1}{3} \lambda^0(31) \lambda^0(42) + \frac{1}{2} \lambda^e(31) \lambda^{eT}(42) \right) f_1 f_2 c_3^+ c_4^+ \left(\frac{4}{9} \lambda^0(31) \lambda^0(42) - \frac{1}{12} \lambda^e(31) \lambda^{eT}(42) \right) \\
& \times c_1 c_2 \chi_{s_q z}^+ \chi_{\bar{s}_{q'} z}^+ G_3(\vec{p}_3) G_4(\vec{p}_4) \left[-\frac{3}{2} - \frac{1}{2} \vec{\sigma}(31) \cdot \vec{\sigma}(42) \right. \\
& + \frac{\vec{\sigma}(42) \cdot \vec{p}'_4 \vec{\sigma}(42) \cdot \vec{p}_2}{8m_q m_{q'}} + \frac{\vec{\sigma}(31) \cdot \vec{p}'_3 \vec{\sigma}(31) \cdot \vec{p}_1}{8m_q m_{q'}} + \frac{3\vec{\sigma}(31) \cdot \vec{p}_1 \vec{\sigma}(42) \cdot \vec{p}_2}{8m_q^2} \\
& - \frac{\vec{\sigma}(31) \cdot \vec{p}_1 \vec{\sigma}(42) \cdot \vec{p}'_4}{8m_q m_{q'}} - \frac{\vec{\sigma}(31) \cdot \vec{p}'_3 \vec{\sigma}(42) \cdot \vec{p}_2}{8m_q m_{q'}} + \frac{3\vec{\sigma}(31) \cdot \vec{p}'_3 \vec{\sigma}(42) \cdot \vec{p}'_4}{8m_{q'}^2} \\
& + \frac{\vec{\sigma}(31) \vec{\sigma}(31) \cdot \vec{p}_1 \vec{\sigma}(42) \vec{\sigma}(42) \cdot \vec{p}_2}{8m_q^2} + \frac{\vec{\sigma}(31) \vec{\sigma}(31) \cdot \vec{p}_1 \vec{\sigma}(42) \cdot \vec{p}'_4 \vec{\sigma}(42)}{8m_q m_{q'}} \\
& + \frac{\vec{\sigma}(31) \cdot \vec{p}'_3 \vec{\sigma}(31) \cdot \vec{\sigma}(42) \vec{\sigma}(42) \cdot \vec{p}_2}{8m_q m_{q'}} + \frac{\vec{\sigma}(31) \cdot \vec{p}'_3 \vec{\sigma}(31) \cdot \vec{\sigma}(42) \cdot \vec{p}'_4 \vec{\sigma}(42)}{8m_{q'}^2} \\
& \left. - \frac{\vec{\sigma}(42) \cdot \vec{p}'_4 \vec{\sigma}(31) \cdot \vec{\sigma}(42) \vec{\sigma}(42) \cdot \vec{p}_2}{8m_q m_{q'}} - \frac{\vec{\sigma}(31) \cdot \vec{p}'_3 \vec{\sigma}(31) \cdot \vec{\sigma}(42) \vec{\sigma}(31) \cdot \vec{p}_1}{8m_q m_{q'}} \right] \\
& \times G_1(\vec{p}_1) G_2(\vec{p}_2) \chi_{s_{qz}} \chi_{\bar{s}_{q'z}}. \tag{A6}
\end{aligned}$$

Then, the potential corresponding to the quark-antiquark annihilation and creation is

$$\begin{aligned}
V_{aq\bar{q}F}(\vec{k}) = & -\frac{g_s^2}{k^2} \left(\frac{1}{3} \lambda_f^0(31) \lambda_f^0(42) + \frac{1}{2} \vec{\lambda}_f(31) \cdot \vec{\lambda}_f^T(42) \right) \\
& \times \left(\frac{4}{9} \lambda^0(31) \lambda^0(42) - \frac{1}{12} \vec{\lambda}(31) \cdot \vec{\lambda}^T(42) \right) \left[-\frac{3}{2} - \frac{1}{2} \vec{\sigma}(31) \cdot \vec{\sigma}(42) \right. \\
& + \frac{\vec{\sigma}(42) \cdot \vec{p}'_4 \vec{\sigma}(42) \cdot \vec{p}_2}{8m_q m_{q'}} + \frac{\vec{\sigma}(31) \cdot \vec{p}'_3 \vec{\sigma}(31) \cdot \vec{p}_1}{8m_q m_{q'}} + \frac{3\vec{\sigma}(31) \cdot \vec{p}_1 \vec{\sigma}(42) \cdot \vec{p}_2}{8m_q^2} \\
& - \frac{\vec{\sigma}(31) \cdot \vec{p}_1 \vec{\sigma}(42) \cdot \vec{p}'_4}{8m_q m_{q'}} - \frac{\vec{\sigma}(31) \cdot \vec{p}'_3 \vec{\sigma}(42) \cdot \vec{p}_2}{8m_q m_{q'}} + \frac{3\vec{\sigma}(31) \cdot \vec{p}'_3 \vec{\sigma}(42) \cdot \vec{p}'_4}{8m_{q'}^2} \\
& + \frac{\vec{\sigma}(31) \vec{\sigma}(31) \cdot \vec{p}_1 \vec{\sigma}(42) \vec{\sigma}(42) \cdot \vec{p}_2}{8m_q^2} + \frac{\vec{\sigma}(31) \vec{\sigma}(31) \cdot \vec{p}_1 \vec{\sigma}(42) \cdot \vec{p}'_4 \vec{\sigma}(42)}{8m_q m_{q'}} \\
& + \frac{\vec{\sigma}(31) \cdot \vec{p}'_3 \vec{\sigma}(31) \cdot \vec{\sigma}(42) \vec{\sigma}(42) \cdot \vec{p}_2}{8m_q m_{q'}} + \frac{\vec{\sigma}(31) \cdot \vec{p}'_3 \vec{\sigma}(31) \vec{\sigma}(42) \cdot \vec{p}'_4 \vec{\sigma}(42)}{8m_{q'}^2} \\
& \left. - \frac{\vec{\sigma}(42) \cdot \vec{p}'_4 \vec{\sigma}(31) \cdot \vec{\sigma}(42) \vec{\sigma}(42) \cdot \vec{p}_2}{8m_q m_{q'}} - \frac{\vec{\sigma}(31) \cdot \vec{p}'_3 \vec{\sigma}(31) \cdot \vec{\sigma}(42) \vec{\sigma}(31) \cdot \vec{p}_1}{8m_q m_{q'}} \right], \tag{A7}
\end{aligned}$$

where the Gell-Mann matrices that operate in flavor space are labeled by the subscript f . $V_{aq\bar{q}F}(\vec{r})$ denoting the Fourier transform of $V_{aq\bar{q}F}(\vec{k})$ is added to $V_{ab}(\vec{r})$ in Eq. (66) to get a potential between a quark and an antiquark. Quark-antiquark relative-motion wave functions are solutions of the Schrödinger equation with the potential $V_{ab}(\vec{r}) + V_{aq\bar{q}F}(\vec{r})$. Keeping only the first two terms enclosed by the brackets, which do not involve quark masses, we get

$$\begin{aligned}
V_{aq\bar{q}F}^0(\vec{k}) = & \frac{g_s^2}{k^2} \left(\frac{1}{3} \lambda_f^0(31) \lambda_f^0(42) + \frac{1}{2} \vec{\lambda}_f(31) \cdot \vec{\lambda}_f^T(42) \right) \\
& \times \left(\frac{4}{9} \lambda^0(31) \lambda^0(42) - \frac{1}{12} \vec{\lambda}(31) \cdot \vec{\lambda}^T(42) \right) \\
& \times \left[\frac{3}{2} + \frac{1}{2} \vec{\sigma}(31) \cdot \vec{\sigma}(42) \right]. \tag{A8}
\end{aligned}$$

In the static limit of quark and antiquark $k^2 \approx (2m_q)^2$ and the corresponding expression in coordinate space is

$$V_{aq\bar{q}F}^0(\vec{r}) = \int \frac{d^3 k}{(2\pi)^3 k^2} \frac{g_s^2}{k^2} \left(\frac{1}{3} \lambda_f^0(31) \lambda_f^0(42) + \frac{1}{2} \vec{\lambda}_f(31) \cdot \vec{\lambda}_f^T(42) \right) \left(\frac{4}{9} \lambda^0(31) \lambda^0(42) - \frac{1}{12} \vec{\lambda}(31) \cdot \vec{\lambda}^T(42) \right) \left[\frac{3}{2} + \frac{1}{2} \vec{\sigma}(31) \cdot \vec{\sigma}(42) \right] e^{i\vec{k}\cdot\vec{r}} \\ = \delta^3(\vec{r}) \frac{g_s^2}{4m_q^2} \left(\frac{1}{3} \lambda_f^0(31) \lambda_f^0(42) + \frac{1}{2} \vec{\lambda}_f(31) \cdot \vec{\lambda}_f^T(42) \right) \left(\frac{4}{9} \lambda^0(31) \lambda^0(42) - \frac{1}{12} \vec{\lambda}(31) \cdot \vec{\lambda}^T(42) \right) \left[\frac{3}{2} + \frac{1}{2} \vec{\sigma}(31) \cdot \vec{\sigma}(42) \right], \quad (\text{A9})$$

which is the annihilation part of the electron-positron potential given in Ref. [62] and of the quark-antiquark potential given in Ref. [3].

Now we begin to apply the expression of $V_{aq\bar{q}F}(\vec{k})$ to get $\mathcal{M}_{aq_1\bar{q}_2}$ and $\mathcal{M}_{a\bar{q}_1q_2}$. For the reaction $A(12) + B(34) \rightarrow C(14) + D(32)$ the initial spin wave function with the total spin S of mesons A and B and its z component S_z is [63]

$$(\chi_A \chi_B)_{S_z}^S = \sum_{S_{13} S_{24}} \hat{S}_A \hat{S}_B \hat{S}_{13} \hat{S}_{24} \begin{Bmatrix} S_1 & S_2 & S_A \\ S_3 & S_4 & S_B \\ S_{13} & S_{24} & S \end{Bmatrix} \times |[(S_1 S_3) S_{13} (S_2 S_4) S_{24}]_{S_z}^S\rangle, \quad (\text{A10})$$

where $\hat{X} = \sqrt{2X+1}$, the two braces indicate the Wigner 9j symbol, χ_A (χ_B) is the spin state of meson A (B), and S_1 , S_2 , S_3 , and S_4 are the spins of particles 1, 2, 3, and 4, respectively. The spin state with the spin S_1 (S_2) and the spin state with the spin S_3 (S_4) are coupled to the spin state

with the spin S_{13} (S_{24}). The spin states with S_{13} and S_{24} are coupled to the spin state vector,

$$|[(S_1 S_3) S_{13} (S_2 S_4) S_{24}]_{S_z}^S\rangle = \sum_{S_{13z} S_{24z}} (S_{13} S_{13z} S_{24} S_{24z} |SS_z\rangle) \times \chi_{S_{13} S_{13z}} \chi_{S_{24} S_{24z}}, \quad (\text{A11})$$

where the Clebsch-Gordan coefficients are used, and S_{13z} and S_{24z} are the z components of S_{13} and S_{24} , respectively. The final spin wave function with the total spin S' of mesons C and D and its z component S'_z is [63]

$$(\chi_C \chi_D)_{S'_z}^{S'} = \sum_{S_{13} S_{42}} \hat{S}_C \hat{S}_D \hat{S}_{13} \hat{S}_{42} \begin{Bmatrix} S_1 & S_4 & S_C \\ S_3 & S_2 & S_D \\ S_{13} & S_{42} & S' \end{Bmatrix} \times |[(S_1 S_3) S_{13} (S_4 S_2) S_{42}]_{S'_z}^{S'}\rangle, \quad (\text{A12})$$

where χ_C (χ_D) is the spin state of meson C (D). The spin states with S_{13} and S_{42} are coupled to the spin state vector,

$$|[(S_1 S_3) S_{13} (S_4 S_2) S_{42}]_{S'_z}^{S'}\rangle = (-1)^{S_{42}-S_4-S_2} \sum_{S_{13z} S_{42z}} (S_{13} S_{13z} S_{42} S_{42z} |S' S'_z\rangle) \chi_{S_{13} S_{13z}} \chi_{S_{42} S_{42z}}. \quad (\text{A13})$$

The spin and spatial part of the initial wave function is [64]

$$\phi_{AB} = (\phi_{A\text{rel}} \chi_A)_{J_{Az}}^{J_A} (\phi_{B\text{rel}} \chi_B)_{J_{Bz}}^{J_B} = \sum_{JJ_z} (J_A J_{Az} J_B J_{Bz} |JJ_z\rangle) \phi_{\text{in}}^{JJ_z}, \quad (\text{A14})$$

where J is the total angular momentum of mesons A and B and J_z is its magnetic projection quantum number. The wave function $\phi_{\text{in}}^{JJ_z}$ is

$$\phi_{\text{in}}^{JJ_z} = [(\phi_{A\text{rel}} \chi_A)^{J_A} (\phi_{B\text{rel}} \chi_B)^{J_B}]_{J_z}^J \\ = \sum_{LS} \hat{J}_A \hat{J}_B \hat{L} \hat{S} \begin{Bmatrix} L_A & S_A & J_A \\ L_B & S_B & J_B \\ L & S & J \end{Bmatrix} [(\phi_{A\text{rel}} \phi_{B\text{rel}})^L (\chi_A \chi_B)^S]_{J_z}^J, \quad (\text{A15})$$

where L_A (L_B) is the orbital angular momentum of meson A (B), L is the total orbital angular momentum of mesons A and B , and

$$[(\phi_{A\text{rel}} \phi_{B\text{rel}})^L (\chi_A \chi_B)^S]_{J_z}^J = \sum_{L_z S_z} (LL_z SS_z |JJ_z\rangle) \times (\phi_{A\text{rel}} \phi_{B\text{rel}})_{L_z}^L (\chi_A \chi_B)_{S_z}^S, \quad (\text{A16})$$

where L_z is the magnetic projection quantum number of L . The spin and spatial part of the final wave function is [64]

$$\phi_{CD} = (\phi_{C\text{rel}} \chi_C)_{J_{Cz}}^{J_C} (\phi_{D\text{rel}} \chi_D)_{J_{Dz}}^{J_D} \\ = \sum_{J' J'_z} (J_C J_{Cz} J_D J_{Dz} |J' J'_z\rangle) \phi_{\text{final}}^{J' J'_z}, \quad (\text{A17})$$

where J' is the total angular momentum of mesons C and D and J'_z is its magnetic projection quantum number. The wave function $\phi_{\text{final}}^{J' J'_z}$ is

$$\begin{aligned} \phi_{\text{final}}^{J'J'_z} &= [(\phi_{C \text{ rel}} \chi_C)^{J_C} (\phi_{D \text{ rel}} \chi_D)^{J_D}]_{J'_z}^{J'} \\ &= \sum_{L'S'} \hat{J}_C \hat{J}_D \hat{L}' \hat{S}' \left\{ \begin{array}{ccc} L_C & S_C & J_C \\ L_D & S_D & J_D \\ L' & S' & J' \end{array} \right\} \\ &\times [(\phi_{C \text{ rel}} \phi_{D \text{ rel}})^{L'} (\chi_C \chi_D)^{S'}]_{J'_z}^{J'}, \end{aligned} \quad (\text{A18})$$

where L_C (L_D) is the orbital angular momentum of meson C (D), L' is the total orbital angular momentum of mesons C and D , and

$$\begin{aligned} [(\phi_{C \text{ rel}} \phi_{D \text{ rel}})^{L'} (\chi_C \chi_D)^{S'}]_{J'_z}^{J'} &= \sum_{L'_z S'_z} (L' L'_z S' S'_z | J' J'_z) \\ &\times (\phi_{C \text{ rel}} \phi_{D \text{ rel}})_{L'_z}^{L'} (\chi_C \chi_D)_{S'_z}^{S'}, \end{aligned} \quad (\text{A19})$$

where L'_z is the magnetic projection quantum number of L' .

Under the Fierz transformations the left diagram in Fig. 1 corresponds to the diagram “T2 prior” in Fig. 4 and the diagram “T2 post” in Fig. 5, where the interacting constituents, q_1 and \bar{q}_2 , are numbered 2 and 4. The transition amplitudes for T2 prior and T2 post are the same and are given by

$$\begin{aligned} \mathcal{M}_{aq_1\bar{q}_2} &= \sqrt{2E_A 2E_B 2E_C 2E_D} \langle \phi_{CD} | \langle CD, I, I_z | \\ &\times \phi_{C \text{ color}}^+ \phi_{D \text{ color}}^+ V_{aq_1\bar{q}_2 F} \phi_{A \text{ color}} \phi_{B \text{ color}} \\ &\times |AB, I, I_z\rangle | \phi_{AB}\rangle. \end{aligned} \quad (\text{A20})$$

We take the following form

$$\begin{aligned} \langle CD, I, I_z | \phi_{C \text{ color}}^+ \phi_{D \text{ color}}^+ V_{aq_1\bar{q}_2 F} \phi_{A \text{ color}} \phi_{B \text{ color}} | AB, I, I_z\rangle \\ = \sum_{n=0}^{15} c_n^{\text{ai}} P_n^{\text{ai}}, \end{aligned} \quad (\text{A21})$$

where $P_0^{\text{ai}} = \sigma_0$, $P_1^{\text{ai}} = \sigma_1(2)$, $P_2^{\text{ai}} = \sigma_2(2)$, $P_3^{\text{ai}} = \sigma_3(2)$, $P_4^{\text{ai}} = \sigma_1(4)$, $P_5^{\text{ai}} = \sigma_2(4)$, $P_6^{\text{ai}} = \sigma_3(4)$, $P_7^{\text{ai}} = \sigma_1(2)\sigma_1(4)$, $P_8^{\text{ai}} = \sigma_1(2)\sigma_2(4)$, $P_9^{\text{ai}} = \sigma_1(2)\sigma_3(4)$, $P_{10}^{\text{ai}} = \sigma_2(2)\sigma_1(4)$, $P_{11}^{\text{ai}} = \sigma_2(2)\sigma_2(4)$, $P_{12}^{\text{ai}} = \sigma_2(2)\sigma_3(4)$, $P_{13}^{\text{ai}} = \sigma_3(2)\sigma_1(4)$, $P_{14}^{\text{ai}} = \sigma_3(2)\sigma_2(4)$, and $P_{15}^{\text{ai}} = \sigma_3(2)\sigma_3(4)$. Here σ_0 is a 2×2 unit matrix. c_n^{ai} ($n = 0, \dots, 15$) are independent of the Pauli matrices, but depend on quark and antiquark momenta. c_n^{ai} include the color matrix element,

$$\phi_{C \text{ color}}^+ \phi_{D \text{ color}}^+ \left(\frac{4}{9} \lambda^0(2) \lambda^0(4) - \frac{1}{12} \vec{\lambda}(2) \cdot \vec{\lambda}^T(4) \right) \phi_{A \text{ color}} \phi_{B \text{ color}},$$

and the flavor matrix element,

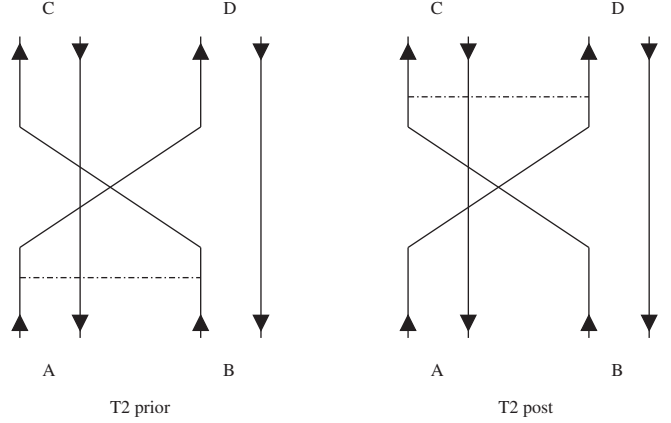


FIG. 17. “prior” and “post” diagrams with quark interchange. Solid (dot-dashed) lines represent quarks or antiquarks (interaction).

$$\langle CD, I, I_z | \left(\frac{1}{3} \lambda_f^0(2) \lambda_f^0(4) + \frac{1}{2} \vec{\lambda}_f(2) \cdot \vec{\lambda}_f^T(4) \right) | AB, I, I_z \rangle.$$

The transition amplitude is thus

$$\mathcal{M}_{aq_1\bar{q}_2} = \sqrt{2E_A 2E_B 2E_C 2E_D} \langle \phi_{CD} | \sum_{n=0}^{15} c_n^{\text{ai}} P_n^{\text{ai}} | \phi_{AB} \rangle. \quad (\text{A22})$$

Under the Fierz transformations the right diagram in Fig. 1 corresponds to the diagrams in Fig. 15, where the interacting constituents, \bar{q}_1 and q_2 , are numbered 1 and 3. The transition amplitudes for the two diagrams are the same and are given by

$$\begin{aligned} \mathcal{M}_{a\bar{q}_1 q_2} &= \sqrt{2E_A 2E_B 2E_C 2E_D} \langle \phi_{CD} | \langle CD, I, I_z | \\ &\times \phi_{C \text{ color}}^+ \phi_{D \text{ color}}^+ V_{a\bar{q}_1 q_2 F} \phi_{A \text{ color}} \phi_{B \text{ color}} | AB, I, I_z \rangle | \phi_{AB} \rangle. \end{aligned} \quad (\text{A23})$$

We take the following form

$$\begin{aligned} \langle CD, I, I_z | \phi_{C \text{ color}}^+ \phi_{D \text{ color}}^+ V_{a\bar{q}_1 q_2 F} \phi_{A \text{ color}} \phi_{B \text{ color}} | AB, I, I_z \rangle \\ = \sum_{n=0}^{15} c_n^{\text{qi}} P_n^{\text{qi}}, \end{aligned} \quad (\text{A24})$$

where $P_0^{\text{qi}} = \sigma_0$, $P_1^{\text{qi}} = \sigma_1(3)$, $P_2^{\text{qi}} = \sigma_2(3)$, $P_3^{\text{qi}} = \sigma_3(3)$, $P_4^{\text{qi}} = \sigma_1(1)$, $P_5^{\text{qi}} = \sigma_2(1)$, $P_6^{\text{qi}} = \sigma_3(1)$, $P_7^{\text{qi}} = \sigma_1(3)\sigma_1(1)$, $P_8^{\text{qi}} = \sigma_1(3)\sigma_2(1)$, $P_9^{\text{qi}} = \sigma_1(3)\sigma_3(1)$, $P_{10}^{\text{qi}} = \sigma_2(3)\sigma_1(1)$, $P_{11}^{\text{qi}} = \sigma_2(3)\sigma_2(1)$, $P_{12}^{\text{qi}} = \sigma_2(3)\sigma_3(1)$, $P_{13}^{\text{qi}} = \sigma_3(3)\sigma_1(1)$, $P_{14}^{\text{qi}} = \sigma_3(3)\sigma_2(1)$, and $P_{15}^{\text{qi}} = \sigma_3(3)\sigma_3(1)$. c_n^{qi} ($n = 0, \dots, 15$) are independent of the Pauli matrices, but rely on quark and antiquark momenta. c_n^{qi} include the color matrix element,

$$\phi_{C\text{color}}^+ \phi_{D\text{color}}^+ \left(\frac{4}{9} \lambda^0(3) \lambda^0(1) - \frac{1}{12} \vec{\lambda}(3) \cdot \vec{\lambda}^T(1) \right) \phi_{A\text{color}} \phi_{B\text{color}}, \quad \mathcal{M}_{a\bar{q}_1 q_2} = \sqrt{2E_A 2E_B 2E_C 2E_D} \langle \phi_{CD} | \sum_{n=0}^{15} c_n^{\text{ai}} P_n^{\text{ai}} + c_n^{\text{qi}} P_n^{\text{qi}} | \phi_{AB} \rangle. \quad (\text{A25})$$

and the flavor matrix element,

$$\langle CD, I, I_z | \left(\frac{1}{3} \lambda_f^0(3) \lambda_f^0(1) + \frac{1}{2} \vec{\lambda}_f(3) \cdot \vec{\lambda}_f^T(1) \right) | AB, I, I_z \rangle.$$

The transition amplitude is thus

The sum of the two transition amplitudes is

$$\mathcal{M}_{a\bar{q}_1 \bar{q}_2} + \mathcal{M}_{a\bar{q}_1 q_2} = \sqrt{2E_A 2E_B 2E_C 2E_D} \langle \phi_{CD} | \sum_{n=0}^{15} (c_n^{\text{ai}} P_n^{\text{ai}} + c_n^{\text{qi}} P_n^{\text{qi}}) | \phi_{AB} \rangle. \quad (\text{A26})$$

Equations (A14)–(A19) yield

$$\begin{aligned} \sum_{J_{Az} J_{Bz} J_{Cz} J_{Dz}} |\mathcal{M}_{a\bar{q}_1 \bar{q}_2} + \mathcal{M}_{a\bar{q}_1 q_2}|^2 &= 16 E_A E_B E_C E_D \sum_{J_{Az} J_{Bz} J_{Cz} J_{Dz}} |\langle \phi_{CD} | \sum_{n=0}^{15} (c_n^{\text{ai}} P_n^{\text{ai}} + c_n^{\text{qi}} P_n^{\text{qi}}) | \phi_{AB} \rangle|^2 \\ &= 16 E_A E_B E_C E_D \sum_{JJ_z J' J'_z} |\langle \phi_{\text{final}}^{J' J'_z} | \sum_{n=0}^{15} (c_n^{\text{ai}} P_n^{\text{ai}} + c_n^{\text{qi}} P_n^{\text{qi}}) | \phi_{\text{in}}^{JJ_z} \rangle|^2, \end{aligned} \quad (\text{A27})$$

where

$$\begin{aligned} \langle \phi_{\text{final}}^{J' J'_z} | \sum_{n=0}^{15} (c_n^{\text{ai}} P_n^{\text{ai}} + c_n^{\text{qi}} P_n^{\text{qi}}) | \phi_{\text{in}}^{JJ_z} \rangle &= \hat{J}_A \hat{J}_B \hat{J}_C \hat{J}_D \sum_{n=0}^{15} \sum_{LSL'S' S_z S'_z} \hat{L} \hat{S} \hat{L}' \hat{S}' \begin{Bmatrix} L_A & S_A & J_A \\ L_B & S_B & J_B \\ L & S & J \end{Bmatrix} \begin{Bmatrix} L_C & S_C & J_C \\ L_D & S_D & J_D \\ L' & S' & J' \end{Bmatrix} \\ &\times (L(J_z - S_z) SS_z | JJ_z) (L'(J'_z - S'_z) S' S'_z | J' J'_z) (\langle \langle (\phi_{C\text{rel}} \phi_{D\text{rel}})^{L'_z - S'_z} | c_n^{\text{ai}} | (\phi_{A\text{rel}} \phi_{B\text{rel}})^{L_z - S_z} \rangle \rangle \\ &\times (\chi_{C\chi_D})_{S'_z}^{S'+} P_n^{\text{ai}} (\chi_{A\chi_B})_{S_z}^S + \langle \langle (\phi_{C\text{rel}} \phi_{D\text{rel}})^{L'_z - S'_z} | c_n^{\text{qi}} | (\phi_{A\text{rel}} \phi_{B\text{rel}})^{L_z - S_z} \rangle \rangle (\chi_{C\chi_D})_{S'_z}^{S'+} P_n^{\text{qi}} (\chi_{A\chi_B})_{S_z}^S). \end{aligned} \quad (\text{A28})$$

The initial spin wave function of mesons *A* and *B* and the final spin wave function of mesons *C* and *D* give the spin matrix elements,

$$\begin{aligned} (\chi_{C\chi_D})_{S'_z}^{S'+} P_n^{\text{ai}} (\chi_{A\chi_B})_{S_z}^S &= \hat{S}_A \hat{S}_B \hat{S}_C \hat{S}_D \sum_{S'_{42} S_{13} S_{24} S_{13z}} (-1)^{S'_{42} - S_4 - S_2} \hat{S}_{13}^2 \hat{S}'_{42} \hat{S}_{24} \begin{Bmatrix} S_1 & S_4 & S_C \\ S_3 & S_2 & S_D \\ S_{13} & S'_{42} & S' \end{Bmatrix} \begin{Bmatrix} S_1 & S_2 & S_A \\ S_3 & S_4 & S_B \\ S_{13} & S_{24} & S \end{Bmatrix} \\ &\times (S_{13} S_{13z} S'_{42} (S'_z - S_{13z}) | S' S'_z) (S_{13} S_{13z} S_{24} (S_z - S_{13z}) | S S_z) \chi_{S'_{42}(S'_z - S_{13z})}^+ P_n^{\text{ai}} \chi_{S_{24}(S_z - S_{13z})}, \end{aligned} \quad (\text{A29})$$

and

$$\begin{aligned} (\chi_{C\chi_D})_{S'_z}^{S'+} P_n^{\text{qi}} (\chi_{A\chi_B})_{S_z}^S &= \hat{S}_A \hat{S}_B \hat{S}_C \hat{S}_D \sum_{S'_{13} S_{13} S_{24} S_{24z}} (-1)^{S_{24} - S_4 - S_2} \hat{S}_{24}^2 \hat{S}'_{13} \hat{S}_{13} \begin{Bmatrix} S_1 & S_4 & S_C \\ S_3 & S_2 & S_D \\ S'_{13} & S_{24} & S' \end{Bmatrix} \begin{Bmatrix} S_1 & S_2 & S_A \\ S_3 & S_4 & S_B \\ S_{13} & S_{24} & S \end{Bmatrix} \\ &\times (S'_{13} (S'_z - S_{24z}) S_{24} S_{24z} | S' S'_z) (S_{13} (S_z - S_{24z}) S_{24} S_{24z} | S S_z) \chi_{S'_{13}(S'_z - S_{24z})}^+ P_n^{\text{qi}} \chi_{S_{24}(S_z - S_{24z})}. \end{aligned} \quad (\text{A30})$$

Similar expressions of the flavor matrix elements are obtained by replacing spin wave functions, spin quantum numbers, P_n^{ai} , and P_n^{qi} in the expressions of the spin matrix elements with flavor wave functions, isospin quantum numbers, $\frac{1}{3} \lambda_f^0(2) \lambda_f^0(4) + \frac{1}{2} \vec{\lambda}_f(2) \cdot \vec{\lambda}_f^T(4)$, and $\frac{1}{3} \lambda_f^0(3) \lambda_f^0(1) + \frac{1}{2} \vec{\lambda}_f(3) \cdot \vec{\lambda}_f^T(1)$, respectively. Using Eqs. (A27)–(A30) in Eq. (34), we obtain the unpolarized cross section.

- [1] Y.-Q. Li and X.-M. Xu, *Nucl. Phys.* **A794**, 210 (2007).
- [2] Z.-Y. Shen and X.-M. Xu, *J. Korean Phys. Soc.* **66**, 754 (2015).
- [3] T. Barnes and E. S. Swanson, *Phys. Rev. D* **46**, 131 (1992); E. S. Swanson, *Ann. Phys. (N.Y.)* **220**, 73 (1992).
- [4] G. E. Brown, C. M. Ko, Z. G. Wu, and L. H. Xia, *Phys. Rev. C* **43**, 1881 (1991).
- [5] S. A. Bass *et al.*, *Prog. Part. Nucl. Phys.* **41**, 255 (1998); C. Nonaka and S. A. Bass, *Phys. Rev. C* **75**, 014902 (2007).
- [6] W. Cassing, E. L. Bratkovskaya, U. Mosel, S. Teis, and A. Sibirtsev, *Nucl. Phys.* **A614**, 415 (1997).
- [7] Y.-Q. Li, X.-M. Xu, and H.-J. Ge, *Eur. Phys. J. A* **47**, 65 (2011).
- [8] M. Kohno and W. Weise, *Nucl. Phys.* **A454**, 429 (1986); **479**, 433c (1988).
- [9] R. Tegen, T. Mizutani, and F. Myhrer, *Phys. Rev. D* **32**, 1672 (1985); F. Myhrer and R. Tegen, *Phys. Lett. B* **162**, 237 (1985).
- [10] J. Haidenbauer, T. Hippchen, and R. Tegen, *Phys. Rev. C* **44**, 1812 (1991); J. Haidenbauer, K. Holinde, V. Mull, and J. Speth, *Phys. Rev. C* **46**, 2158 (1992).
- [11] C. B. Dover and P. M. Fishbane, *Nucl. Phys.* **B244**, 349 (1984); *Phys. Rev. Lett.* **62**, 2917 (1989).
- [12] M. Maruyama, S. Furui, and A. Faessler, *Nucl. Phys.* **A472**, 643 (1987); A. Muham, T. Gutsche, R. Thierauf, Y. Yan, and A. Faessler, *Nucl. Phys.* **A598**, 285 (1996).
- [13] T. Muta, *Foundations of Quantum Chromodynamics* (World Scientific, Singapore, 1987).
- [14] See Supplemental Material at <http://link.aps.org/supplemental/10.1103/PhysRevD.94.034030> for a method to study inelastic meson-meson scattering that is governed by quark-antiquark annihilation and creation. The transition potential for the quark-antiquark annihilation and creation is derived in perturbative QCD. Unpolarized cross sections are obtained from the transition amplitude that contains color, spin, and flavor matrix elements. Prominent temperature dependence of the cross sections is found.
- [15] S.-T. Ji, Z.-Y. Shen, and X.-M. Xu, *J. Phys. G* **42**, 095110 (2015).
- [16] W. Buchmüller and S.-H. H. Tye, *Phys. Rev. D* **24**, 132 (1981).
- [17] F. Karsch, E. Laermann, and A. Peikert, *Nucl. Phys.* **B605**, 579 (2001).
- [18] Z. V. Chraplyvy, *Phys. Rev.* **91**, 388 (1953); **92**, 1310 (1953).
- [19] M. A. Stroscio, *Phys. Rep.* **22C**, 215 (1975).
- [20] A. De Rújula, H. Georgi, and S. L. Glashow, *Phys. Rev. D* **12**, 147 (1975).
- [21] X.-M. Xu, *Nucl. Phys.* **A697**, 825 (2002).
- [22] S. Godfrey and N. Isgur, *Phys. Rev. D* **32**, 189 (1985).
- [23] K. Nakamura *et al.* (Particle Data Group), *J. Phys. G* **37**, 075021 (2010).
- [24] E. Colton, E. Malamud, P. E. Schlein, A. D. Johnson, V. J. Stenger, and P. G. Wohlmuth, *Phys. Rev. D* **3**, 2028 (1971).
- [25] N. B. Durusoy, M. Baubillier, R. George, M. Goldberg, A. M. Touchard, N. Armenise, M. T. Fogli-Muciaccia, and A. Silvestri, *Phys. Lett. B* **45**, 517 (1973).
- [26] M. J. Losty, V. Chaloupka, A. Ferrando, L. Montanet, E. Paul, D. Yaffe, A. Ziemiński, J. Alitti, B. Gandois, and J. Louie, *Nucl. Phys.* **B69**, 185 (1974).
- [27] W. Hoogland *et al.*, *Nucl. Phys.* **B126**, 109 (1977).
- [28] S. D. Protopopescu, M. Alston-Garnjost, A. Barbaro-Galtieri, S. M. Flatté, J. H. Friedman, T. A. Lasinski, G. R. Lynch, M. S. Rabin, and F. T. Solmitz, *Phys. Rev. D* **7**, 1279 (1973).
- [29] B. Hyams *et al.*, *Nucl. Phys.* **B64**, 134 (1973).
- [30] P. Estabrooks and A. D. Martin, *Nucl. Phys.* **B79**, 301 (1974).
- [31] V. Srinivasan *et al.*, *Phys. Rev. D* **12**, 681 (1975).
- [32] L. Rosselet *et al.*, *Phys. Rev. D* **15**, 574 (1977).
- [33] C. D. Froggatt and J. L. Petersen, *Nucl. Phys.* **B129**, 89 (1977).
- [34] A. A. Bel'kov, S. A. Bunyatov, K. N. Mukhin, O. O. Patarakin, V. M. Sidorov, M. M. Sulkovskaya, A. F. Sustavov, and V. A. Yarba, *JETP Lett.* **29**, 597 (1979).
- [35] E. A. Alekseeva, A. A. Kartamyshev, V. K. Makar'in, K. N. Mukhin, O. O. Patarakin, M. M. Sulkovskaya, A. F. Sustavov, L. V. Surkova, and L. A. Chernysheva, *Sov. Phys. JETP* **55**, 591 (1982).
- [36] R. García-Martín, R. Kamiński, J. R. Peláez, J. R. de Elvira, and F. J. Ynduráin, *Phys. Rev. D* **83**, 074004 (2011).
- [37] N. F. Mott and H. S. W. Massey, *The Theory of Atomic Collisions* (Clarendon Press, Oxford, 1965).
- [38] T. Barnes, N. Black, and E. S. Swanson, *Phys. Rev. C* **63**, 025204 (2001).
- [39] C.-Y. Wong and H. W. Crater, *Phys. Rev. C* **63**, 044907 (2001).
- [40] J. Gasser and H. Leutwyler, *Ann. Phys. (N.Y.)* **158**, 142 (1984); *Nucl. Phys.* **B250**, 465 (1985).
- [41] J. Gasser and U. G. Meissner, *Phys. Lett. B* **258**, 219 (1991); *Nucl. Phys.* **B357**, 90 (1991).
- [42] J. V. Steele, H. Yamagishi, and I. Zahed, *Nucl. Phys.* **A615**, 305 (1997).
- [43] T. N. Truong, *Phys. Rev. Lett.* **61**, 2526 (1988); A. Dobado, M. J. Herrero, and T. N. Truong, *Phys. Lett. B* **235**, 134 (1990); S. Willenbrock, *Phys. Rev. D* **43**, 1710 (1991).
- [44] A. Dobado and J. R. Peláez, *Phys. Lett. B* **286**, 136 (1992); A. Dobado and J. Morales, *Phys. Rev. D* **52**, 2878 (1995).
- [45] G. F. Chew and S. Mandelstam, *Phys. Rev.* **119**, 467 (1960); J. A. Oller and E. Oset, *Phys. Rev. D* **60**, 074023 (1999); M. Albaladejo, J. A. Oller, and L. Roca, *Phys. Rev. D* **82**, 094019 (2010).
- [46] T. N. Truong, *Phys. Rev. Lett.* **67**, 2260 (1991); A. Dobado and J. R. Peláez, *Phys. Rev. D* **47**, 4883 (1993); T. Hannah, *Phys. Rev. D* **55**, 5613 (1997); A. Dobado and J. R. Peláez, *Phys. Rev. D* **56**, 3057 (1997); M. Boglione and M. R. Pennington, *Z. Phys. C* **75**, 113 (1997); J. Nieves, M. P. Valderrama, and E. R. Arriola, *Phys. Rev. D* **65**, 036002 (2002).
- [47] B. S. Zou and D. V. Bugg, *Phys. Rev. D* **48**, R3948 (1993); **50**, 591 (1994); F. Q. Wu, B. S. Zou, L. Li, and D. V. Bugg, *Nucl. Phys.* **A735**, 111 (2004).
- [48] J. S. Borges, J. S. Barbosa, and V. Oguri, *Phys. Lett. B* **393**, 413 (1997).
- [49] B. Ananthanarayan and P. Büttiker, *Phys. Lett. B* **415**, 402 (1997); B. Ananthanarayan, *Phys. Rev. D* **58**, 036002 (1998).
- [50] J. A. Oller and E. Oset, *Nucl. Phys.* **A620**, 438 (1997); J. A. Oller, E. Oset, and J. R. Peláez, *Phys. Rev. Lett.* **80**, 3452 (1998); *Phys. Rev. D* **59**, 074001 (1999).
- [51] J. Nieves and E. R. Arriola, *Phys. Lett. B* **455**, 30 (1999).

- [52] G. Janssen, B. C. Pearce, K. Holinde, and J. Speth, *Phys. Rev. D* **52**, 2690 (1995).
- [53] B. A. Li, *Phys. Rev. D* **52**, 5165 (1995).
- [54] Y. B. He, J. Hüfner, S. P. Klevansky, and P. Rehberg, *Nucl. Phys. A* **630**, 719 (1998).
- [55] H. Chen, *Phys. Rev. D* **80**, 034029 (2009).
- [56] R. García-Martín and B. Moussallam, *Eur. Phys. J. C* **70**, 155 (2010).
- [57] I. V. Danilkin, L. I. R. Gil, and M. F. M. Lutz, *Phys. Lett. B* **703**, 504 (2011).
- [58] N. N. Achasov and A. V. Kiselev, *Phys. Rev. D* **83**, 054008 (2011).
- [59] M. Albaladejo, J. A. Oller, E. Oset, G. Rios, and L. Roca, *J. High Energy Phys.* **08** (2012) 071.
- [60] H. J. Weber, *Ann. Phys. (N.Y.)* **177**, 38 (1987).
- [61] B. L. G. Bakker, M. Bozoian, J. N. Maslow, and H. J. Weber, *Phys. Rev. C* **25**, 1134 (1982).
- [62] V. B. Berestetskii, E. M. Lifshitz, and L. P. Pitaevskii, *Quantum Electrodynamics* (Elsevier Ltd., Oxford, 1982).
- [63] R. D. Lawson, *Theory of the Nuclear Shell Model* (Clarendon Press, Oxford, 1980).
- [64] C.-Y. Wong, E. S. Swanson, and T. Barnes, *Phys. Rev. C* **65**, 014903 (2001).